Cellulose
https://doi.org/10.1007/s10570-024-05839-3

ORIGINAL RESEARCH

Antibacterial *Komagataeibacter hansenii* nanocellulose membranes with avocado seed bioactive compounds

Kaja Kupnik · Mateja Primožič · Vanja Kokol · Željko Knez · Maja Leitgeb

Received: 24 October 2023 / Accepted: 2 March 2024

Abstract Biocompatible, mechanically stable, highly hydrophilic/swellable and safe antibacterial biomaterials are crucial for wound dressing and other applications in the health sector. Therefore, this study was conducted for the development of bacterial nanocellulose membranes, which were, for the first time, enriched with bacteriostatic and bactericidal effective avocado seed extracts prepared by different extraction techniques (ultrasonic, Soxhlet, high pressure with supercritical carbon dioxide). First, the production process of bacterial nanocellulose membranes from *Komagataeibacter hansenii* bacteria was optimized related to the fermentation media composition and culture conditions, resulting in bacterial nanocellulose membranes with up to 83% crystallinity and 54.5 g/L yield. The morphological structure of the membranes was varied further by using air- and freeze-drying processes. The Soxhlet and high pressure with supercritical carbon dioxide avocado seed extracts with the most charge negative surface (-33 mV) and smallest hydrodynamic size (0.1 µm) thus resulted in 100% reduction of both Gram-negative *Escherichia coli* and Gram-positive *Staphylococcus aureus* with up to log reduction of 2.56 and up to 100% bactericidal efficacy after 24 h of exposure, and at 14 mg/g of avocado seed extracts integrated in the bacterial nanocellulose membranes homogeneously. The high swelling (up to 600%) and water retention ability of avocado seed extracts enriched bacterial nanocellulose membranes, with a biocidal release up to 2.71 mg/mL, shows potential for antibacterial applications in the biomedicine, cosmetics, and pharmaceutical industries.

Keywords Bacterial nanocellulose membrane · Avocado seed extracts · Extraction · Swelling · Release · Antibacterial activity

K. Kupnik · M. Primožič · Ž. Knez · M. Leitgeb (✉)
Faculty of Chemistry and Chemical Engineering, University of Maribor, Smetanova ulica 17, 2000 Maribor, Slovenia
e-mail: maja.leitgeb@um.si

K. Kupnik
e-mail: kaja.kupnik@um.si

M. Primožič
e-mail: mateja.primozic@um.si

Ž. Knez
e-mail: zeljko.knez@um.si

K. Kupnik · V. Kokol
Faculty of Mechanical Engineering, University of Maribor, Smetanova ulica 17, 2000 Maribor, Slovenia
e-mail: vanja.kokol@um.si

Ž. Knez · M. Leitgeb
Faculty of Medicine, University of Maribor, Taborska ulica 8, 2000 Maribor, Slovenia

Introduction

Bacterial nanocellulose (BNC) is biosynthesized mostly by acetic acid bacteria (e.g., *Komagataeibacter hansenii*), where, during the fermentation, the

Published online: 02 April 2024

bacterial cells first secrete nanocellulose chains which assemble and aggregate, and then bundle into nanocellulose ribbons. Aerobic bacteria are known for their active motility, hence, under static conditions, BNC membrane (BNCM) is formed at the liquid–air interface (Ullah et al. 2019). Depending on the biosynthesized conditions, BNCM exhibit a wide range of remarkable physico-chemical properties, including ultrafine, porous morphology with a high specific surface area, advantageous mechanical properties, high crystallinity and water holding capacity. Besides, it's intrinsically high purity and biocompatibility, nontoxicity, and bio-degradability, provide applications in cosmetics, pharmacy, and biomedicine (Ullah et al. 2016; Khine and Stenzel 2020; Kupnik et al. 2020; Mbituyimana et al. 2021). Its application in the delivery of drugs to a wound in the form of a mono/multilayer film, membrane or capsule shells to inhibit external microbial infections (Czaja et al. 2006; Jipa et al. 2012; Lazarini et al. 2016; Ullah et al. 2017), as a stabilizer (Shen et al. 2023), a hydrogel carrier (Yi et al. 2023), and as a scaffold in the form of the aerogel (Zhou et al. 2021) has already been investigated well.

Microbial infections and the upsurge in antimicrobial resistance (AMR) is recognized as a top concern and a severe threat to the global economy and public health by various health agencies (e.g., the World Health Organization (WHO), Centers for Disease Control and Prevention (CDC), the European Medical Agency (EMA)) (Bhattacharjee et al. 2023). In this context, the primary strategy has become to endow biomaterials with antibacterial properties. Considering all the advantageous features of BNC, that, nevertheless, lacks the antimicrobial capacity (Li et al. 2017), different antimicrobial substances, including nanoparticles, biomolecules, and natural or synthetic polymers, have been introduced into it (Sulaeva et al. 2015) and studied for different applications.

Currently, a large number of scientific articles report on the applications of BNC-based composites, enriched with plant extracts, while the ever-increasing push for a circular economy has led to a widespread research in reusing fruit waste (Campos et al. 2020). In this frame, BNC has already been enriched with extracts from oregano, rosemary, parsley, lovage (Bodea et al. 2022), green tea and henna leaves (Pooja et al. 2019; Azarmi et al. 2022), roselle flower petals (Indrianingsih et al. 2020), propolis (Mocanu et al. 2019; Amorim et al. 2022), dragon tree (Kamal et al. 2022), sunflower, annatto, barbatimao, pink lapacho, marigold (Neves et al. 2022), and fireweed (Perużyńska et al. 2023). Fruit wastes have been studied in abundance for increased yield and higher quality of BNC production (Urbina et al. 2021), but only two studies with extracts of pomegranate peels (Ul-Islam et al. 2023) and mangosteen peels (Taokaew et al. 2014) have been detected in the literature for the purpose of achieving biological activity of modified BNC. No studies on BNC enrichment with avocado extract have been reported yet.

The health-promoting benefits of avocado (*Persea americana*) fruit are certainly a dominant drawing card for consumers all over the world. Global avocado production expanded to over 8.4 m millions metric tons in 2022 and at a compound annual growth rate (CAGR) of about 7% during the last decade (Rabobank 2023). Due to the large production and avocado consumption, and the fact that an avocado seed can represent up to 26% of the entire fruit weight, there is a huge amount of waste generated (Domínguez et al. 2016). The chemical composition and bioactivity of selected compounds from avocado seeds is already well known (Bangar et al. 2022; Kupnik et al. 2023; Sánchez-Quezada et al. 2023). Avocado seed extracts (ASE) are rich in polyphenols, acetogenins, fatty acids, triterpenoids, and other compounds that exhibit excellent antimicrobial, antioxidant, antihypertensive, hypolipidemic, and larvicidal activities (Leite et al. 2009; Nwaoguikpe et al. 2011; Jimenez et al. 2021). It was noticed that the content of biologically active compounds is influenced extremely by the choice of extraction method and the selected solvent, as we have shown in our latest study (Kupnik et al. 2023). In general, ASE have been shown to be excellent growth inhibitors of some Gram-negative (G-), Gram-positive (G+) bacteria, and selected fungi. The detected high contents of hesperidin, vanillin and 2,3-dihydroxybenzoic acid in ASE contributed to the excellent antimicrobial efficiency, while the high activity of the enzyme superoxide dismutase (SOD) strengthened its antioxidant potential additionally (Kupnik et al. 2023). All the obtained ASE exhibited promising results in terms of biological activity, but it is necessary to emphasize that the ASE obtained with modern, greener, and more sustainable supercritical fluid extraction (SFE),

has resulted the highest content of proteins and phenols (Kupnik et al. 2023).

The aim of this study was thus to prepare BNCMs enriched with ASE obtained by different extraction techniques, and evaluate their antibacterial properties. First, a comprehensive study was carried out to optimize the cultivation conditions for production of BNCMs by *K. hansenii* bacteria to achieve the highest possible yield. Then, the influence of cultivation time on the mass, thickness, cellulose content and crystallinity of BNCMs was evaluated. In addition, the influence of different drying methods, i.e., air and freeze-drying, was carried out to evaluate their morphology and swelling. In the next step, BNCMs were enriched with ASE prepared by different extraction methods. The antibacterial efficiency, bacteriostatic and bactericidal activity of BNCMs enriched with ASE were evaluated on G- *Escherichia coli* and G + *Staphylococcus aureus*. To explain and interpret possible mechanisms of antibacterial activity against different bacteria, the ASE were characterized by surface charge and hydrodynamic size, while also determining potential ASE release after 24 h of exposure. The swelling and water retention capacity of BNCMs, as well as their chemical structure and morphology, were also studied, to evaluate their further applications in biomedicine, cosmetics, and pharmaceutics. To the best of our knowledge, this is the first study investigating the physico-chemical properties, morphology, and antibacterial activity of BNCMs enriched with ASE comprehensively, comparing the ASE prepared by different extraction methods (ultrasonic/US, Soxhlet/SE, and supercritical fluid/SFE).

Experimental

Chemicals and microbial strains used

Dimethyl sulfoxide (DMSO, ≥ 99.5%) was purchased from Kemika, Zagreb, Croatia. Citric acid (≥ 99.5%), D-(+)-glucose anhydrous (≥ 97.5%), di-sodium hydrogen phosphate (Na_2HPO_4, ≥ 99.0%), ethanol (EtOH, ≥ 99.5%), and peptone were purchased from Merck, Darmstadt, Germany. Carbon dioxide (CO_2, purity 2.5) was purchased from Messer, Ruše, Slovenia. Acetic acid (glacial, ≥ 99.7%), agar, sodium hydroxide (NaOH, ≥ 95.0%), sucrose, and yeast extract were purchased from Sigma-Aldrich, St. Louis, USA, while the Mueller–Hinton broth was from Biolife, Milano, Italy. All chemicals were used without further purification. The selected microorganisms (*K. hansenii* (DSM 5602), *E. coli* (DSM 498), and *S. aureus* (DSM 346)) were purchased from DSMZ-German Collection of Microorganisms and Cell Cultures GmbH from Berlin, Germany.

Media, culture conditions and production of BNCMs

The well-known complex Hestrin and Schramm (HS) medium (Urbina et al. 2021) was selected as the growth medium, which was prepared as follows: 20 g/L glucose, 5 g/L peptone, 5 g/L yeast extract, 1.15 g/L citric acid and 2.7 g/L Na_2HPO_4.

HS medium was also selected as a production medium, and further, optimization of the media and culture conditions was carried out using a single-variable optimization method. In order to obtain the highest BNCM yield, glucose and sucrose were tested as carbon sources. Furthermore, the concentration (2, 4, or 6% w/v) of the added carbon source was optimized, followed by the concentration (0.5, 2, or 4% w/v) of peptone as a nitrogen source. In addition, different pH values (5.5, 6.0, and 6.5) of the medium were also tested, to achieve the highest possible yield of BNCMs` production. All the experiments were performed in triplicates.

One loopful of *K. hansenii* was inoculated in 50 mL of growth HS medium, and grown at 27 ± 1 °C on a rotary shaker (150 rpm) for 48 h. The resulting suspension was used as an inoculum (5% v/v, $1–5 \times 10^6$ CFU/mL) for the next experiments. The inoculated flasks were incubated under static conditions at 27 ± 1 °C for 21 days to obtain BNCMs. After cultivation and production, the prepared BNCMs were harvested from the production medium, washed thoroughly with distilled water, and immersed in 1 *N* NaOH solution at 80 ± 5 °C for 2 h to remove the bacterial cells and medium components embedded in the membranes. Lastly, the BNCMs were soaked and rinsed repeatedly with distilled water until a neutral pH was attained in the washed liquid. The BNCMs` production yield was measured as the wet weight of BNCM recalculated per volume of the culture medium [g/L].

Evaluation of the BNCMs` wet mass, thickness, and dry weight cellulose content

The influence was studied of different incubation times (7, 14, 21, 28, and 35 days) on the BNCMs` production. The BNCMs` mass was measured in a wet state, and its thickness was evaluated at different points (i.e., near the edges and at central positions) using a digital micrometer (3109 Series, INSIZE Co., Ltd, Spain); the values are presented as an average of 10 obtained points (±Standard Deviation/SD). Furthermore, the BNCMs were frozen at around -18 °C, and then lyophilized in a Mini Lyotrap laboratory freeze drying unit (LTE Scientific Ltd., UK) for about 48 h, and reweighed. The dry mass of cellulose content was calculated from the following equation:

$$Dry\ Mass\ Cellulose\ Content\ [\%] = \frac{m_{dry\ BNCM}}{m_{wet\ BNCM}} \times 100 \quad (1)$$

where $m_{dry\ BNCM}$ and $m_{wet\ BNCM}$ denote the weight of BNCM before ($m_{wet\ BNCM}$) and after ($m_{dry\ BNCM}$) the drying process, respectively. All the experiments were performed in triplicates, and the results are reported as mean value ± SD.

Effect of the drying method on the structure of the BNCMs

Two different drying methods were used to evaluate and compare the morphology of the obtained BNCMs. According to the air-drying method, the BNCMs were air dried until they reached a constant mass under controlled conditions (temperature of 20 ± 2 °C and 65 ± 5% humidity). In the case of the freeze-drying method, the samples were frozen at around -18 °C, and then lyophilized in a Mini Lyotrap laboratory freeze drying unit (LTE Scientific Ltd., UK) for about 48 h. About 96.39 ± 0.10% of water was removed by both drying techniques.

X-ray diffraction (XRD) analysis of the BNCMs

The crystallinity of the BNCMs was characterized by XRD collected on a Bruker D2 Phaser (MA, USA) diffractometer with Cu Kα radiation (λ = 1.54 Å) at 30 kV and 10 mA. Scattered radiation was detected in the range of 2θ from 5 to 70° at a scan rate of 0.3 s/step. The crystallinity index (C_I) was calculated using the following equation, developed by Segal and coworkers (Segal et al. 1959):

$$C_I\ [\%] = \frac{I_{110} - I_{AM}}{I_{110}} \times 100 \quad (2)$$

where I_{AM} and I_{110} denote, respectively, the intensity of diffraction pattern at 2θ around 18° corresponding to the amorphous regions in the cellulose, and the intensity of the diffraction peak at 2θ = 22.7° which is associated with the crystalline region of cellulose (French and Santiago Cintrón 2013; French 2014; Singhsa et al. 2018).

Using Bragg equation, the d-spacing of cellulose samples was calculated:

$$d\ [nm] = \frac{n\lambda}{2 \sin \theta} \quad (3)$$

where n denote order of reflection, λ is the wavelength of the X-ray source (0.154 nm) and θ is the Bragg angle corresponding to the plane. In order to determine the dominant crystal allomorph (I_α or I_β) in different BNCMs samples, the calculation by Wada (Wada et al. 2001) was adopted. This calculation proposes the function applied to discriminate between the I_α and I_β rich types:

$$Z = 1693 d_1 - 902 d_2 - 549 \quad (4)$$

where d_1 and d_2 denote, respectively, the d-spacing of (100) plane and the d-spacing of (010) plane. If Z > 0, the BNCM is classified as I_α rich, while Z < 0 indicate I_β rich type.

Scanning electron microscopy (SEM) imaging of the BNCMs

The morphology of the dried BNCMs was examined by a high-resolution FEI Sirion 400NC microscope (FEI, Hillsboro, OR, USA). Approximately 1 cm^2 pieces of dried BNCMs were cut, placed on a holder and sputtered with a gold to ensure conductivity and prevent charging effects.

Preparation of the ASE

The obtained avocado seeds (Hass variety) and further ASE were prepared by different extraction

methods, as detailed in our publication (Kupnik et al. 2023). Briefly, ultrasound extraction (US) was performed for 3 h at 20 °C and 40 kHz, using H_2O as a solvent. Soxhlet extraction (SE) with ethanol (EtOH) as a solvent was carried out for four recycles to be completed, while supercritical fluid extraction (SFE) was conducted for 2 h at 40 °C and 20 MPa, using CO_2 (2 mL/min) as a solvent and EtOH (0.5–0.8 mL/min) as co-solvent. The solvents were evaporated with a rotary evaporator (Büchi Rotavapor R-114, Flawil, Switzerland) at 40 °C and reduced pressure. All the obtained ASE were stored at around -20 °C before their further usage.

Dynamic light scattering (DLS) analysis of ASE

The hydrodynamic size and zeta potential (ZP) of the ASE at a concentration of 0.05 wt% (dispersed in milliQ), were assessed at 25 ± 0.1 °C by DLS using a Zetasizer Nano ZS ZEN360 (Malvern Instruments Ltd., Malvern, UK). The DTS1070 disposable folded capillary cell was used, implementing the following parameters: a dispersion refractive index of 1.330 (milli-Q H_2O) and a viscosity of 0.8872 cP (milli-Q H_2O). A field of 150 V was implemented across the nominal electrode spacing of 16 mm. The samples (1 mL) were measured immediately after being dispersed at 10.000 rpm for 3 min using an Ultra-turrax T25 (IKA GmbH, Staufen, Germany). At least six individual measurements were performed, and the mean values ± SD were calculated.

Modification of the BNCMs with ASE

For modification of the BNCMs, the ASE obtained via different extraction methods were dispersed individually in sterilized deionized water (dH_2O) or a 5% (v/v) DMSO solution, to prepare 1 or 10 wt% concentrated ASE solutions, respectively. The exhaust method (Sakthivel et al. 2016; Sharma and Bhardwaj 2019) was applied, which is based on the transfer of bioactive compounds from the bulk medium (i.e., the ASE solutions) to the surface of the substrate (i.e., the BNCMs) and further diffusion into the substrate. For that purpose, the wet BNCMs were simply immersed in different ASE solutions for 48 h. The magnetic stirrer (Tehtnica Rotamix 550 MMH, Železniki, Slovenia) of 150 rpm was used to facilitate diffusion of the ASE into the BNCMs. After adsorption, the modified BNCMs enriched with ASE were taken out and soaked over a filter paper to remove the excess extract.

Attenuated total reflectance–fourier transform infrared (ATR-FTIR) analysis of BNCMs enriched with ASE

The ATR-FTIR was employed for chemical characterization of differently ASE enriched BNCMs. Approximately 1 cm^2 pieces of dried samples were used for recording the spectrum. The IR spectra were performed using a Perkin-Elmer spectrum one FTIR spectrometer (Waltham, MA, USA) with ATR crystal accessories at ambient conditions, and a 4 cm^{-1} resolution from collecting 16 scans per spectrum for each sample at a region of 4000–450 cm^{-1}. The air spectrum subtraction and background were performed in parallel. The Spectrum 5.0.2 software was used for the data analysis. All the measurements were performed in duplicate.

Antibacterial activity of BNCMs enriched with ASE

To assess the antibacterial ability qualitatively against the G- *E. coli* and G + *S. aureus* of the prepared BNCMs, the agar diffusion assay was applied, following the protocol described in our previous studies (Kupnik et al. 2021a, b) with slight modifications. The BNCMs were exposed to UV light overnight before testing to avoid possible contamination. 100 µL of the prepared bacteria solution ($1–5 \times 10^6$ CFU/mL) was spread evenly over Mueller–Hinton agar plates. Then, approx. 1 cm^2 pieces of sterilized BNCMs were put directly on the inoculated agar plates. The incubation of the inoculated agar plates took place under optimal growth conditions for both bacteria (37 ± 1 °C for 24 h). The unmodified/pure BNCMs were taken as a control in each case. The results are reported as the diameter (in mm) of the inhibition zone formed around the samples. All the experiments were performed in triplicates, and the results are reported as the mean value ± SD.

The bacteriostatic and bactericidal activity of the modified BNCMs with ASE were assessed using the plate count method. The BNCMs were exposed to UV irradiation overnight to avoid possible contamination. The sterilized approx. 1 cm^2 pieces of BNCMs were

put into the test tubes containing 10 mL of bacterial suspension with the concentration of 1–5 × 10^6 CFU/mL and incubated under optimal growth conditions for both bacteria (37 ± 1 °C for 24 h). After incubation, 100 µL of the final and serially diluted bacterial suspensions were spread over the Mueller–Hinton agar plates and incubated for 24 h at 37 ± 1 °C. The number of colonies were counted under a colony counter (PBI F4, Milano, Italy). The antibacterial activity of BNCMs enriched with ASE was determined by calculating the log reduction factor (log R), the percentage of reduction (R), and bactericidal efficacy using the following equations:

$$Log\ Reduction\ Factor\ [\%] = log_{10}(\frac{S_p}{S_m}) \quad (5)$$

$$Bacterial\ Reduction\ Rate\ [\%] = \frac{S_p - S_m}{S_p} \times 100 \quad (6)$$

$$Bacterial\ Killing\ Efficacy\ [\%] = \frac{CFU_c - CFU_s}{CFU_c} \times 100 \quad (7)$$

where S_p and S_m denote, respectively, the number of viable bacterial colonies from pure BNCM (unmodified) and the number of viable bacterial colonies from modified (ASE reach) BNCM. The CFU_c value signifies the number of colonies forming units per mL of the control sample (no BNCM sample added, only *E. coli* or *S. aureus*), and the CFU_s value means the number of colony forming units per mL of BNCMs enriched with ASE. All the experiments were performed in triplicates, and results are reported as the mean value ± SD.

Swelling and water retention properties of BNCMs enriched with ASE

To determine the swelling ratio (SR), dried BNCMs with ASE (in size of approx. 2 cm^2) were weighed ($m_{dry\ BNCM}$) and immersed into 50 mL of dH_2O. After specific time periods, the BNCMs were weighed ($m_{wet\ BNCM}$) after removing the surface water by filter paper. To assess the water retention (WR) capacity, the dried BNCMs enriched with ASE were weighed ($m_{dry\ BNCM}$), and then soaked into dH_2O for 24 h. The BNCMs were taken out, whipped witha filter paper to remove the surface water, and placed on an open plate to evaluate the water retention. The weights of the BNCMs ($m_{wet\ BNCM}$) were measured at certain time periods. The WR and SR were determined using the following equation (Lin et al. 2013b):

$$WR\ or\ SR\ [\%] = \frac{m_{wet\ BNCM} - m_{dry\ BNCM}}{m_{dry\ BNCM}} \times 100 \quad (8)$$

where $m_{wet\ BNCM}$ and $m_{dry\ BNCM}$ denote, respectively, the weight of the wet BNCM and the weight of the dried BNCM. All the experiments were performed in triplicates, and results are reported as the mean value.

Release of ASE from BNCMs

To determine the release of different ASE from the prepared BNCMs, wet and air-dried BNCMs enriched with ASE (in size of approx. 1 cm^2, wet weight of approx. 0.2 g) were placed in a vial containing 5 mL of dH_2O at 37 ± 1 °C with constant stirring (100 rpm). After 24 h, the amount (mg/mL) of released ASE was monitored using a UV–VIS spectrophotometer, and determined using pre-prepared calibration curves for the dilution series of the corresponding ASE.

Results and discussion

Optimization of cultivation conditions for BNCMs` production

Komagataeibacter (formerly *Gluconacetobacter* or *Acetobacter*) is well known in the production of BNC, but cultivation conditions vary with the strains. *K. hansenii* is characterized by a very high cellulose production rate (Bimmer et al. 2023) and high crystallinity (Güzel and Akpınar 2020), therefore, it was used and tested for optimal production in a complex HS medium and under static culture conditions (Sperotto et al. 2021) by varying nutritional (e.g., the source and concentration of carbon and nitrogen) and physical (e.g. pH) parameters. The studied parameters` influence and obtained production yield of BNCM are summarized in Table 1. When the glucose and sucrose were compared in terms of their efficiencies in the production yield of BNCM, the sucrose was more efficient, resulting in 15.48 ± 1.86 g/L, compared to 13.54 ± 1.39 g/L BNCMs with glucose. It was already established by other studies that, for some isolates, sucrose can

Table 1 Influence of different growing parameters on BNCM production by *K. hansenii* in HS medium at 27 ± 1 °C after 21 days

Parameters	Carbon source	Carbon source concentration [w/v%]	Nitrogen source concentration [w/v%]	pH	BNCM yield [g/L ± SD]
Production medium (unmodified HS medium)	Glucose	2	0.5	6.0	12.65 ± 2.14
Carbon source	Glucose	2			13.54 ± 1.39
	Sucrose				15.48 ± 1.86
Sucrose concentration (w/v)%	Sucrose	2			/
		4			45.49 ± 3.98
		6			18.35 ± 2.71
Nitrogen source concentration (w/v)%	Sucrose	4	0.5		/
			2		51.86 ± 4.22
			4		26.31 ± 8.67
pH	Sucrose	4	2	5.5	10.66 ± 1.82
				6	54.48 ± 4.08
				6.5	31.52 ± 3.56
Optimal cultivation parameters	Sucrose	4	2	6	54.48 ± 4.08

serve as the best carbon source for high production of BNC, and that after reaching the optimal concentration, the yield of BNC production begins to decrease with increasing the concentration of the carbon source (Zeng et al. 2011; Rani and Appaiah 2011). However, according to the literature (Keshk and Sameshima 2005; Pourramezan et al. 2009; Mohite et al. 2013) 2 w/v% of sucrose added to the culture medium shell resulted in the most effective production. On the contrary, in our case, the addition of 2 w/v% of sucrose did not result in the formation of BNCMs, while the addition of 4 w/v% resulted in an almost 2.5 times higher production yield (45.49 ± 3.98 g/L) than by adding 6 w/v% of sucrose. As peptone and yeast extract are preferred nitrogen sources and the basic components of the complex medium (Sperotto et al. 2021), the effect of peptone concentration was evaluated on the BNCMs` production yield. It was observed that the lowest tested concentration (0.5 w/v%) did not result in the formation of BNCMs, while a 2 w/v% concentration of peptone gave a 2 times higher BNCM yield (51.86 ± 4.22 g/L) compared to 4 w/v%. The optimal pH range for BNCMs` production for *Acetobacter* sp. was found to be between 4.0–7.0 (Fontana et al. 1990), while it differed between the strains and variables on the culture conditions. It is considered that most strains produce BNCMs most effectively in the pH range of 5.0–6.0 (Lima et al. 2017; Cielecka et al. 2020, 2021), which is in agreement with our study. When applying static conditions, it is important to note that the pH value decreases during cultivation (usually to pH 3.5) because of the respiratory metabolism of bacteria (Lin et al. 2013a). The initial pH value of 6.0 was demonstrated to be optimal for *K. hansenii,* as the BNCM production yield was as much as 5.1 times higher (54.48 ± 4.08 g/L) than at pH 5.5 (10.66 ± 1.82 g/L), and approx. 1.7 times higher than at pH 6.5 (31.52 ± 3.56 g/L). As compared to other studies (Rani and Appaiah 2011; Uzyol and Saçan 2017), the initial pH value is very important for bacterial cell growth and high BNC production. The HS fermentation medium modified with 4 w/v% of sucrose and 2 w/v% of peptone at an initial pH of 6.0 was thus optimal medium for *K. hansenii* and provided the highest BNCM yield (54.48 ± 4.08 g/L). The purified BNCM obtained under optimal growth conditions is shown in Fig. 1b.

After obtaining the optimal cultivation conditions for the production of BNCMs, different cultivation times have been evaluated in terms of the BNCMs` physical characteristics. Based on visual appearance, after 7 days of fermentation the BNCM had not yet formed, while, after 14 days, a visible thin layer had already started to form at the air–liquid interface. According to other studies (Mikkelsen et al. 2009; Ruka et al. 2012), sucrose requires an additional metabolic step to catalyze sucrose into fructose and glucose itself. Therefore, in the sucrose-based medium, initially, low levels of cellulose are produced, and, after a longer time, the levels of cellulose increase,

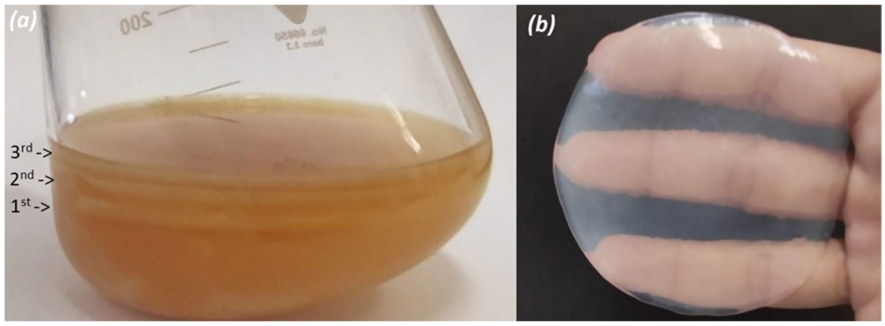

Fig. 1 **a** BNCMs after 35 days of cultivation in HS medium at 27 °C resulting in the formation of 3 layer membranes (1st, 2nd, 3rd) (**b**) Purified BNCM after 21 days of cultivation in HS medium using 4 w/v% of sucrose and 2 w/v% of peptone at pH 6.0 and 27 ± 1 °C

due to an increased lag period for cellulose production. The 1st compact BNCM was visible after 21 days of cultivation. Interestingly, after 28 days of fermentation, two layered BNCMs were formed, while, after 35 days, 3 layered BNCMs were present in the Erlenmeyer flasks, as shown in Fig. 1a.

The multiple layers of BNCMs were thought to be caused by the formation of a new membrane due to the preceding membrane sinking. At the beginning of cultivation, the fermentation medium provides full nutritional value, yet the bacterial concentration is very low at that time and the BNCM starts to form slowly. Further, as the BNCM is formed at the air–liquid interface, its thickness and mass increase, so the first BNCM may sink with time. The formation of a BNCM is related directly to the surface at the air–liquid interface. When the concentration of bacterial cells is high and the nutrient value of the cultivation medium remains adequate and sufficient, the sub-fibrils of cellulose are extruded constantly from the linearly ordered pores at the surface of the bacteria. These then crystallize into microfibrils, and form intertwined and overlapping cellulose ribbons, forming disorganized, parallel planes. Hence, on the surface of the medium the cellulose can assemble into a new BNCM (Auta et al. 2017; Wang et al. 2019).

As illustrated in Fig. 2, the cultivation time certainly has an influence on all the studied characteristics of BNCMs. The first important factor is the BNCMs` overall yield (Fig. 2a). It was 1.9 and 1.2 times higher (117.8 ± 9.67 g/L) after 35 days of cultivation than after 21 (63.18 ± 7.46 g/L) and 28 (96.31 ± 8.13 g/L) days. The masses of the 1st BNCMs were comparable, ranging from 6.214 ± 0.918 g to 6.475 ± 0.431 g. The mass of the 2nd and 3rd BNCMs, which were formed after a longer cultivation time, decreased, which can be attributed to less nutritional fermentation medium. A similar trend can also be detected in the thickness (Fig. 2b) and cellulose content (Fig. 2c). The maximum thickness was reached by the 1st BNCMs (up to 1.876 ± 0.243 mm), while the thickness of the 3rd BNCM after 35 days was determined as 0.483 ± 0.152 mm. Similarly, the cellulose content ranged in-between 2.998 ± 0.241 and 3.203 ± 0.137 wt% in the 1st BNCMs, while the 2nd and 3rd formed BNCMs reached only half the cellulose content (up to 1.631 ± 0.121 wt%) compared to the 1st one.

The diffractograms of the so biosynthesized BNCMs, presented in Fig. 2d, confirmed the formation of a semi-crystalline structure of cellulose I, which was composed of amorphous and crystalline regions that occur in two distinct allomorphs, I_α and I_β, respectively (Atalla and VanderHart 1984). The more intense and sharper peak means higher crystallinity of the sample (Khamrai et al. 2017). All the diffractograms depict three main diffraction signals at 2θ of around 14.6°, 16.8°, and 22.7°, thus corresponding to a cellulose I_α one-chain triclinic unit cell with Miller indices for the peaks of 100, 010, and 110, which coincided with the peaks $1\ \bar{1}\ 0$, 110, and 200 of cellulose I_β (French 2014). As reported (Aleshina et al. 2019; Heydorn et al. 2023), diffraction signals at around 20.5° are assigned to multiple overlapping I_α crystalline signals $11\ \bar{2}$, $01\ \bar{2}$, and $10\ \bar{2}$. In addition, it is necessary to discuss the XRD pattern of BNCM after 21 days of cultivation, where additional peaks that are not from cellulosic material were observed. As can be seen from the literature (George et al. 2008; Sheykhnazari et al. 2011; Mohammadkazemi et al. 2015b; Fan et al. 2016), additional peaks can be attributed to components from the culture media and may be present due to not thoroughly purified BNCM sample. Thus, the components of the culture medium

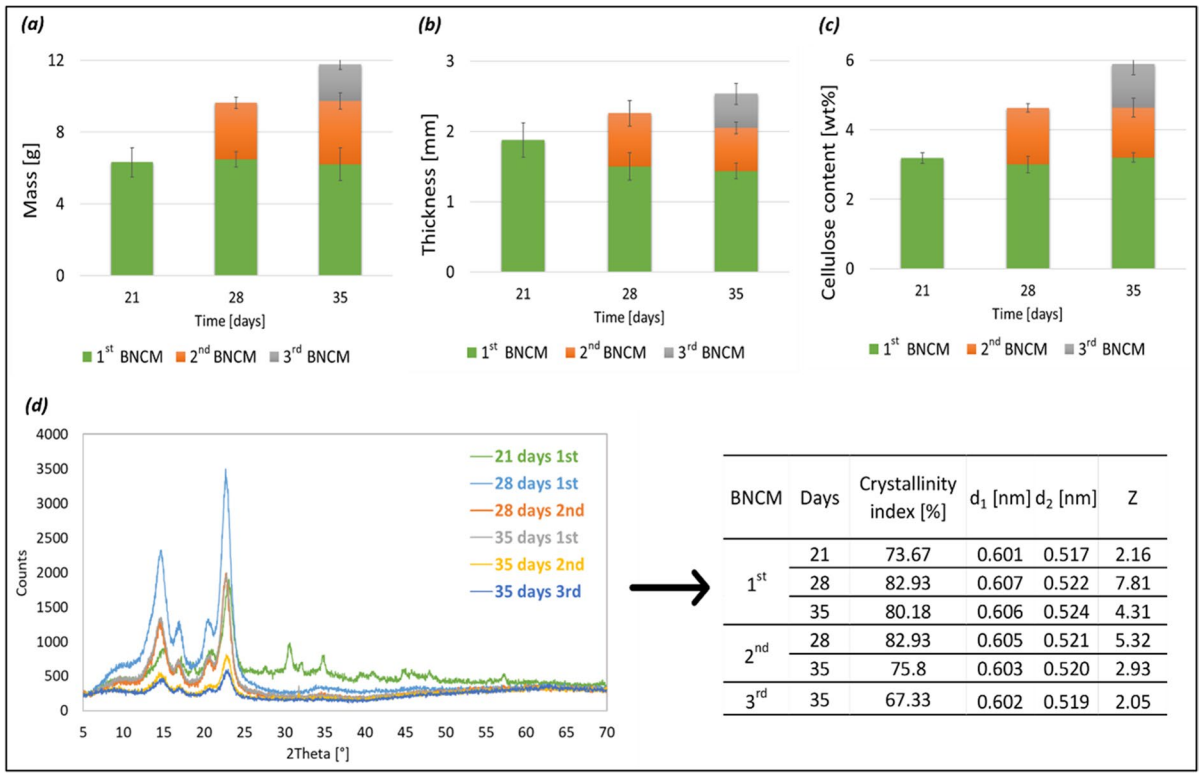

BNCM	Days	Crystallinity index [%]	d_1 [nm]	d_2 [nm]	Z
1st	21	73.67	0.601	0.517	2.16
	28	82.93	0.607	0.522	7.81
	35	80.18	0.606	0.524	4.31
2nd	28	82.93	0.605	0.521	5.32
	35	75.8	0.603	0.520	2.93
3rd	35	67.33	0.602	0.519	2.05

Fig. 2 Effect of *K. hansenii* cultivation time in HS medium at 27 ± 1 °C on the (**a**) mass, (**b**) thickness, (**c**) cellulose content, and (**d**) XRD patterns of the formed BNCMs with crystallinity index (C_I), d-spacing and Z values

can interfere with the aggregation of BNC fibrils, which in turn lowers the crystallinity. In particular, the presence of a peak at 2θ around 19° could slightly interfere with that at around 18° corresponding to the amorphous region in the cellulose and used to calculate crystallinity index (C_I) in Segal equation. Due to the co-existing peak positions of I_α and I_β allomorphs, it is difficult to differentiate between them by determining only the XRD peak positions. Nevertheless, from d-spacing, the Z values (Fig. 2, inserted table) were calculated according to a method described by Wada (Wada et al. 2001). Calculated values enable the dominant classification of cellulose I_α (when $Z > 0$, triclinic form) and I_β (when $Z < 0$, monoclinic form). Presented results imply the domination of the triclinic structure (I_α type) in all BNCMs, regarding the Z values between 2.05 and 7.81. It was also observed that the higher the crystallinity, the higher the Z value was, indicating a higher domination of I_α-rich type cellulose in BNCMs. Previous results also confirmed that cellulose produced by bacteria and algae is predominantly enriched with I_α crystalline phase (Digel et al. 2023). However, a higher intensity of peak at around 14.6°, as that at around 16.8°, indicates the preferred orientation of crystalline segments in the membranes, due to the reflection mode on the X-ray diffractometer. According to the literature (Fang and Catchmark 2014), observation of the BNCMs in transmission mode with the incident X-ray beam from perpendicular to the membrane surface would show an inverted ratio of the mentioned peaks. Furthermore, the calculated crystallinity values fell within the range of 67.33–82.93%. The highest crystallinity was observed for both BNCMs harvested after 28 fermentation days, and its slight decreasing after further production. The results are in line with other studies (Sheykhnazari et al. 2011), indicating that the bacterial strain, media composition and fermentation time used had a great impact on its degree (Dayal et al. 2013). For comparison, cultivation of *K. hansenii* in HS medium resulted in a crystallinity of 58% (Cielecka et al. 2021), cultivation of

G. xylinus on sucrose resulted in BNC with a crystallinity of 63.2% (Mohammadkazemi et al. 2015a), while the crystallinity of the BNC produced by different *Komagataeibacter* strains emerged in the range of 64–80% (Vigentini et al. 2019; Gupte et al. 2021) and in the range of 73–90%, depending on the choice of carbon source (Wang et al. 2018).

Effect of the drying method on the BNCMs` microstructure and ASE integration

Air-drying and freeze-drying methods were applied in order to obtain BNCMs with different microstructure, fibrils entanglement/arrangement, water absorption capacity, and accessibility of hydroxyl groups (Pinto et al. 2012; Hu et al. 2014; Zeng et al. 2014) for an effective integration (diffusion and interaction) of ASE. Figure 3 depicts air-dried BNCM (a) and freeze-dried BNCM (b) with corresponding SEM images of the surface (c, d) and cross-sections (e, f). It can be seen that the drying method had no important influence on the surface structure, while there is a difference in their cross-sections. Both cross-section images of the BNCMs show a layered fibrillated structure, although, when the BNCM was air-dried, the thermodynamically slow moisture removal resulted in shrinkage due to irreversible interactions (i.e., hydrogen bonds) (Fatima et al. 2022) and thus the formation of a compact, denser and more homogeneous structure with high adhesion between the fibrils (Fig. 3e). On the other hand, the freeze-dried BNCM resulted in a well-oriented, but more open and micro-porous network with a less dense nature (Fig. 3f), similar to a previous report (Illa et al. 2019),

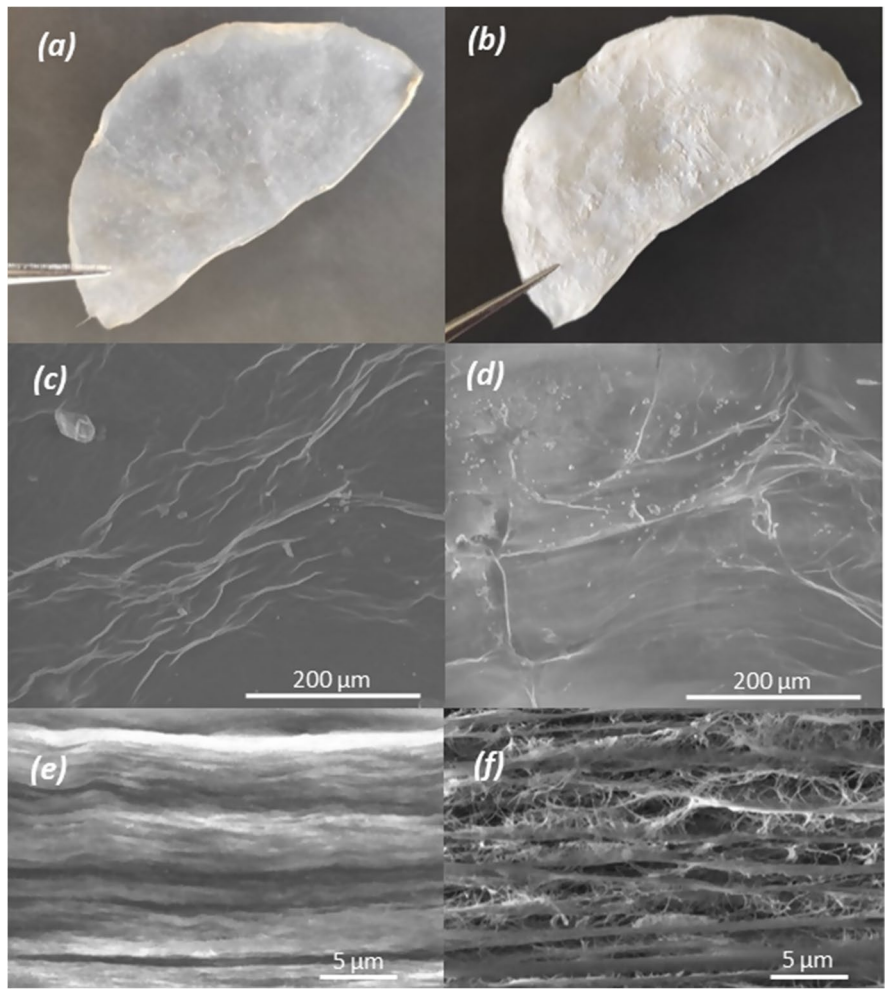

Fig. 3 **a** Air-dried and **(b)** freeze-dried (optimally produced) BNCMs visualized by SEM imaging on their surfaces (**c** and **d**; voltage 15.0 kV, magnification 500x), and in the cross-sections (**e** and **f**; voltage 15.0 kV, magnification 10000x)

corresponding to the creation of ice-crystals from water molecules at the contact points where cryogelation occurs (Tang et al. 2010).

During the development of modified BNCMs (Fig. 4a) through the ex-situ exhaust method, the solutions, suspended particles, and pure liquid diffused into the porous BNCM network and interacted with the available hydroxyl groups by inter- and intramolecular hydrogen bonding interactions. The nature of additives and their particle size are main factors that can influence the degree of penetration/diffusion and attachment greatly. Figure 5 presents the SEM images of BNCMs enriched with 1 wt% of differently extracted ASE. The traces of dried ASE attached to the fibrils` surface are visible, and appear as layers in the BNCMs` network structure. The SOX-EtOH (Fig. 5c) and $scCO_2$ + EtOH (Fig. 5d) extracted ASE are incorporated homogeneously throughout the densely packed air-dried BNCMs. On the contrary, US-H_2O ASE (Fig. 5b) particles accumulated and integrated in the BNCMs, both on the surface and in the bulk (as seen from the cross-sections of the BNCMs), which can most likely be explained by the poorer dispersibility of this type of extract, in line with results from its hydrodynamic size (Table 2). The remarkably hydrodynamically larger in size (around 1.34 µm) and highly polydisperzed (PDI of 0.65) US-H_2O ASE are visible from the SEM micrographs, while they cannot be observed in case of the much smaller (0.1–0.11 µm) and size-homogeneous (PDI of 0.17–0.14) SOX-EtOH and $scCO_2$ + EtOH ASE enriched BNCMs. However, the morphological features, in aspect of layered fibrillated homogenous structure with open and micro-porous network, of BNCMs enriched with ASE are comparable with pure BNCM.

The FTIR spectral profiles of the freeze-dried BNCMs were analyzed to provide an insight on the alteration of the BNCMs` chemical composition and interactions after the incorporation of ASE. As seen from Fig. 4b, all the spectra exhibited characteristic absorption bands of pure bacterial cellulose, i.e. peaks at 3270–3280 cm^{-1} (O–H stretching), 2920 cm^{-1} (C-H stretching of alkane and asymmetric CH_2 stretching), 1640 cm^{-1} (H–O-H bending band of adsorbed H_2O), 1500 cm^{-1} (CH_2 groups), 1450 cm^{-1} (H-C-H and O-C-H stretching of carbonyl groups), 1160 cm^{-1} (C–O–C stretching), 1035–1060 cm^{-1} (C-O stretching) (Ghozali et al. 2021). No significant difference between the FTIR spectra of differently dried BNCMs can be detected, which suggests that the drying process did not change the intermolecular

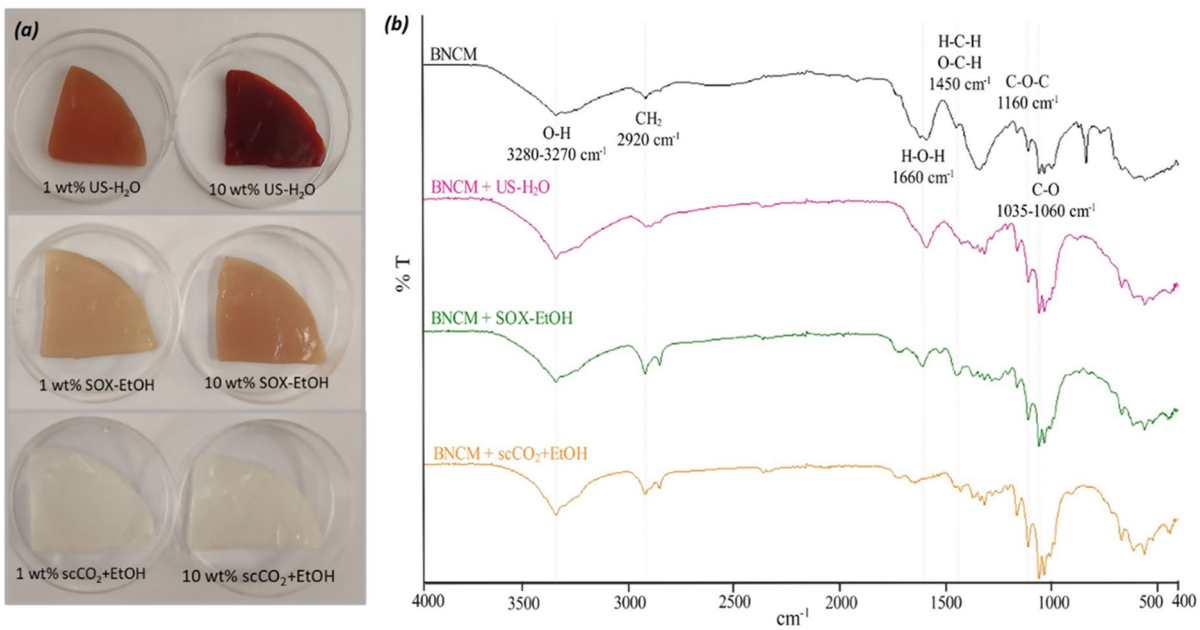

Fig. 4 **a** Photo images of wet BNCMs enriched with different concentrations (1 and 10 wt%) of ASE, obtained by US-H_2O, SOX-EtOH, and $scCO_2$ + EtOH extractions, and corresponding **(b)** ATR-FTIR spectra of freeze-dried samples

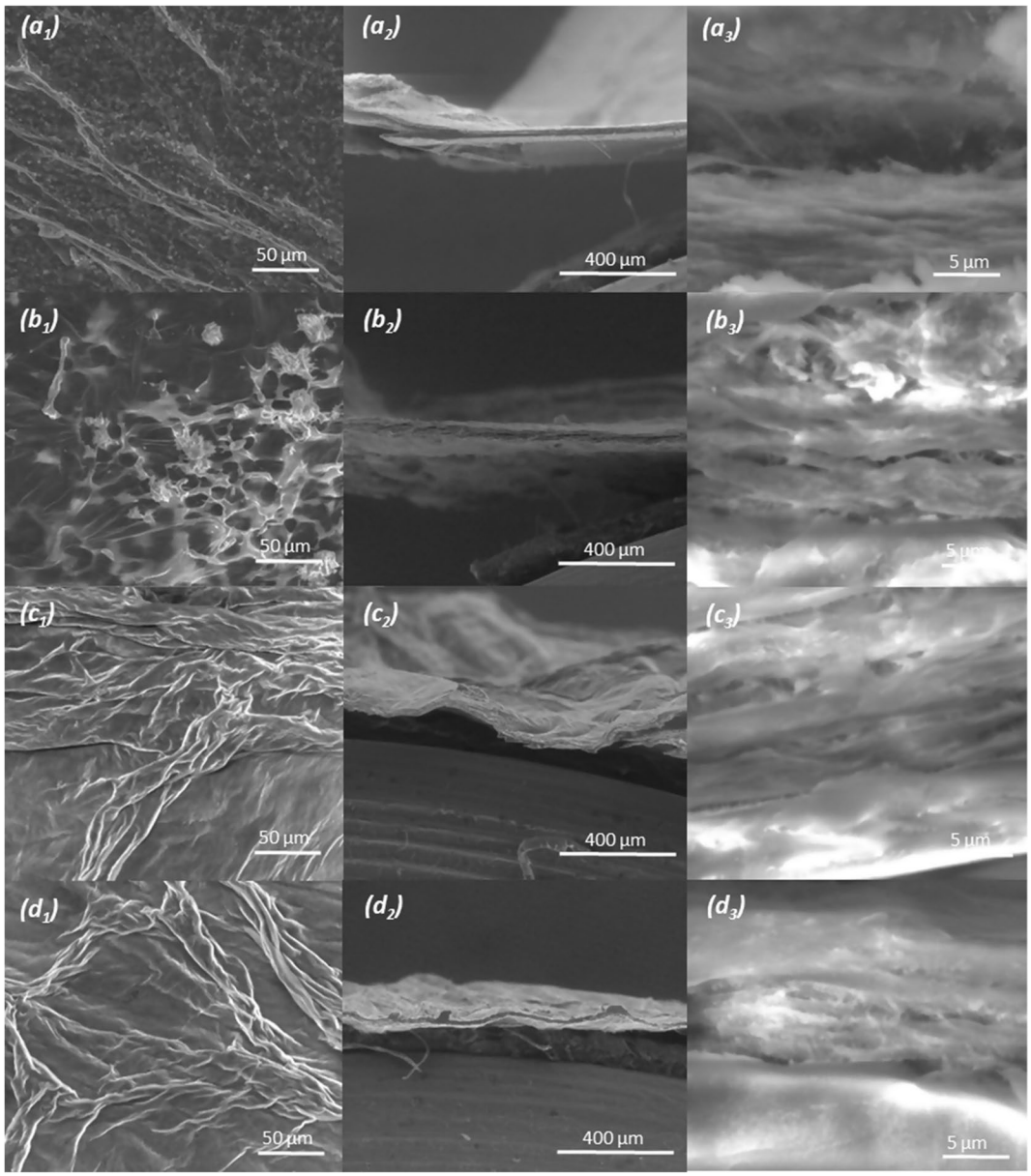

Fig. 5 SEM images of freeze-dried (**a**) pure BNCM and BNCMs enriched with (**b**) US-H_2O, (**c**) SOX-EtOH, and (**d**) $scCO_2$ + EtOH extracts with the concentration of 1 wt%. Subscripts 1 indicate the surface of the BNCMs (voltage 15.0 kV; magnification 200x), while 2 (voltage 15.0 kV; magnification 200x) and 3 (voltage 15.0 kV; magnification 5000x) indicate the cross-sections of the BNCMs enriched with ASE

composition of the BNCMs, which is in agreement with the results of other authors (Mohamad et al. 2022).

The presence of ASE did not result in the appearance of many specific spectral characteristics that could be attributed to the molecular structure of ASE. The peak at 3343 cm^{-1} is present in all the spectra, and could be assigned to the stretching vibration of the -OH bonds in the cellulose (Yassine et al. 2016). The mentioned absorption band is more intense for BNCMs enriched with ASE compared to pure BNCM, as it can be associated to the vibration of the -OH

Table 2 Zeta potential, hydrodynamic size and polydisperse index of 0.05 wt% ASE, as well as their MIC_{90} values after 24 h (Kupnik et al. 2023)

ASE	Zeta potential [mV]	Hydrodynamic size [nm]	Polydispersity index	MIC_{90} [mg/mL]	
				E. coli G- bacterium	*S. aureus* G + bacterium
US-H_2O	-22.2 ± 1.3	1340.7 ± 363.6	0.65 ± 0.14	0.21	2.78
SOX-EtOH	-34.3 ± 2.9	100.1 ± 1.2	0.17 ± 0.01	0.28	0.21
$scCO_2$ + EtOH	-33.1 ± 3.7	114.7 ± 1.6	0.14 ± 0.02	0.21	0.28

stretching in alcohols, carboxylic acids, and phenols (Rodríguez et al. 2016) from ASE. The higher intensity of bands around 2930 cm^{-1} for BNCMs enriched with SOX-EtOH and $scCO_2$ + EtOH ASE may correspond to the CH_3 or CH_2 vibrations of carboxylic acids, such as salicylic acid (Neves et al. 2022). This is in accordance with our already published results (Kupnik et al. 2023), where salicylic acid was determined in both the mentioned extracts, but not in US-H_2O ASE. The band at 1640–1600 cm^{-1} could be due to the stretching vibration of C = C, aromatic ring deformations, asymmetric bending vibration of N–H and stretching vibration of C = O and C = C from flavonoids and amino acids, and C = O stretching from caffeic acid (Oliveira et al. 2016). The bands between 1280 and 1274 cm^{-1} could be attributed to the C–C-O group of phenolic compounds and C-O vibration of -OH of flavonoids (Neves et al. 2022). According to the literature, absorption bands in the spectra of BNCMs enriched with ASE at 3343 cm^{-1}, around 2930 cm^{-1}, between 1315–1360 cm^{-1} and at approx. 1030 cm^{-1} may correspond to the -OH stretching band, H-C-H symmetric stretching of alkanes, N = O asymmetric stretching (nitrate), C–C-N symmetric/asymmetric bending and C-N stretching, respectively, which are characteristic peaks for phytochemicals from ASE (Bogireddy and Agarwal 2019).

Swelling and water retention properties of BNCMs enriched with ASE

The drug or extract release activity (kinetic) from the materials can be influenced by many factors, including drug/extract concentration, its physicochemical characteristics (size and surface chemistry), the kinetic of release and solubility/dispersibility in the surrounding media (environment), as well as the swelling properties of the material (Kalkhoran et al. 2018). Therefore, BNCMs enriched with ASE were evaluated for swelling (SW) and water retention (WR) properties, while also determining their release after 24 h of exposure. The results of SR and WR are shown in Fig. 6. The gravimetric method determined that, in the case of BNCMs` immersion in 1 or 10 wt% solution of ASE, an average of 1.46 ± 0.69 mg and 14.05 ± 4.21 mg of ASE per 1 g of wet BNCM were incorporated, respectively, regardless of the chosen extraction method. Furthermore, the release of the extracts, determined by a spectrophotometric method, was found to be of 85.76 ± 6.89 (from air-dried BNCMs) and 95.62 ± 2.71% (from wet BNCMs), respectively.

The modifications in the physical appearance of BNCMs are likely to bring changes to their physical characteristics. The SR and WR are the most important properties which are connected directly in the biomedical wound dressing applications (Islam et al. 2012). The proper moist environment can promote the release of antibacterial substances, therefore, it provides protection against contamination, while, on the other hand, ensures a proper wound moisture by adsorbing and retaining it, which accelerates the healing procedure and enables a painless and easy dressing change without damage to the healed or newly formed skin (Shezad et al. 2010). The results from the presented study indicate that all BNCMs were able to absorb a high amount of water. The SW of pure BNCM and BNCMs enriched with ASE were around 600 and 490–530%, respectively, comparable, as reported earlier, for bacterial cellulose hydrogels (i.e., 400–600% SR) (Treesuppharat et al. 2017). It can be inferred that the integrated extracts leads to a lowering of the SR, which can be attributed to the hydrogen bonding interaction between the phytomolecules

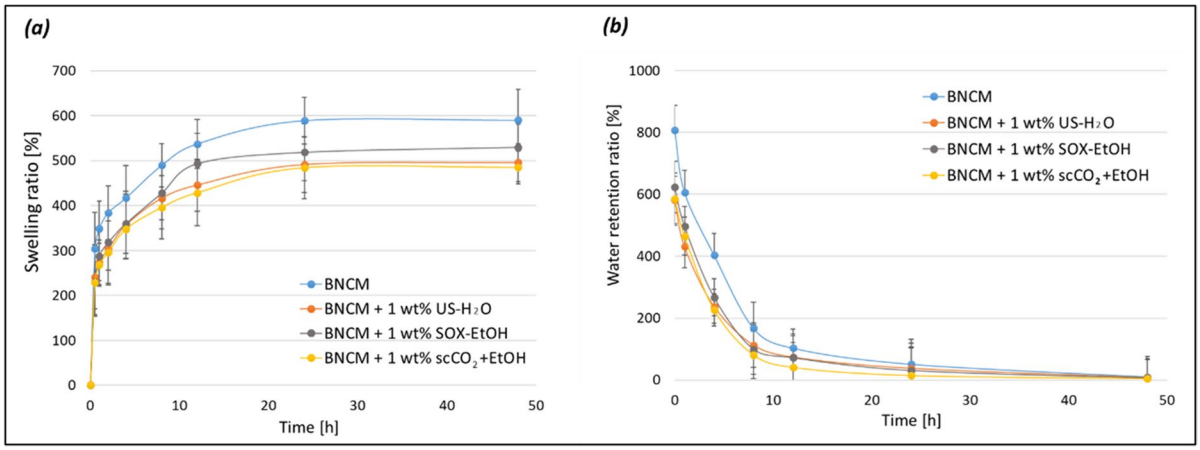

Fig. 6 **a** Swelling ratio (SR) and **(b)** Water retention (WR) rate of air-dried pure BNCM and BNCMs enriched with ASE (extracted by US-H_2O, SOX-EtOH, and $scCO_2$ + EtOH processes) concentration of 1 wt%

of ASE and the OH groups on the cellulose surface, blocking the availability of cellulosic hydroxyl groups for water adsorption (Ul-Islam et al. 2023), as evidenced from the FTIR analysis. On the other hand, this also depends on the arrangement of its microstructure, as closely arranged fibrils bind water molecules more efficiently because of the stronger hydrogen bonding interactions (Shezad et al. 2010; Islam et al. 2012), thus resulting in quantitatively lower ASE adsorption, as well as their release. In the case of pure BNCM and BNCMs enriched with ASE it took about 48 h for the near complete evaporation of the adsorbed water. When comparing the results of BNCMs with differently extracted ASE, the sample containing ASE prepared by $scCO_2$ gave kinetically the lowest SW as well as WR, which can be related to the hydrodynamically smaller ASE particles interacting more extensively with the fibrillated structure, which slows down the adsorption of water and its excretion. As reported earlier for BNCMs enriched with natural antibacterial agents (Lin et al. 2013b), it can be concluded that BNCMs enriched with ASE maintain a suitable moisture environment for wound healing applications for low- to mid-range exudates.

Antibacterial activity of BNCMs enriched with ASE

Until now, no studies have been detected in the reviewed literature with the enrichment of BNCMs with ASE for the purposes of antibacterial efficacy for further applications. Therefore, the presented study is the first reporting the antibacterial effectiveness of the prepared BNCMs, the influence of differently prepared extracts on their antibacterial activity against G- *E. coli* and G + *S. aureus* (as already confirmed in our previous research (Kupnik et al. 2023) given MIC_{90} between 210–280 µg/mL for *E.coli* and 140–2780 µg/mL for *S. aures*; Table 2) and, further, on BNCMs enriched with ASE, providing additional information and insight for potential applications.

The qualitative agar diffusion method was used to evaluate the antibacterial efficiency of BNCMs enriched with ASE, and the results are shown in Table 3 and Fig. 7.

The growth of both G- *E. coli* and G + *S. aureus* was inhibited effectively by BNCMs immersed in highly concentrated 10 wt% ASE solutions, due to the consequent higher adsorption of extracts (around 14.05 mg/g vs. 1.46 mg/g), and, therefore, also 10 times higher release (around 30.1 mg/mL vs. 0.30 mg/mL). BNCMs with 1 wt% US-H_2O ASE did not inhibit the growth of any of the tested bacteria, while the addition of 1 wt% SOX-EtOH ASE inhibited both bacteria by 17 ± 3 mm. BNCMs with the addition of 10 wt% ASE solutions proved to be good growth inhibitors of both the tested bacteria, with inhibition zones formed in the range between 13 ± 2 and 26 ± 1 mm. BNCMs enriched with $scCO_2$ + EtOH ASE proved to be the most promising antibacterial agents, due to the best results compared to BNCMs modified with US-H_2O and SOX-EtOH ASE. Besides, the difference in the inhibition of bacteria

Table 3 Qualitatively determined antimicrobial activity of BNCMs enriched with different ASE concentrations against G- *E. coli* and G + *S. aureus*, swelling ratio (SW), and release of ASE from wet and air-dried BNCMs after 24 h

BNCM enriched with differently extracted ASE	ASE [wt%]	Inhibition zone[mm]		Swelling ratio (24 h) [%]	Release (24 h) [mg/mL]	
		E. coli G- bacterium	*S. aureus* G + bacterium		Wet BNCM	Air-dried BNCM
US-H_2O	1	-	-	491.18 ± 61.74	0.27 ± 0.02	0.27 ± 0.04
	10	13 ± 2	15 ± 2	475.04 ± 58.32	2.71 ± 0.19	2.60 ± 0.20
SOX-EtOH	1	17 ± 3	17 ± 1	519.03 ± 62.54	0.26 ± 0.06	0.25 ± 0.09
	10	18 ± 3	21 ± 1	n.d	n.d	n.d
$scCO_2$ + EtOH	1	23 ± 2	16 ± 3	484.33 ± 79.12	0.41 ± 0.07	0.31 ± 0.07
	10	26 ± 1	18 ± 3	n.d	n.d	n.d

n.d. not determined

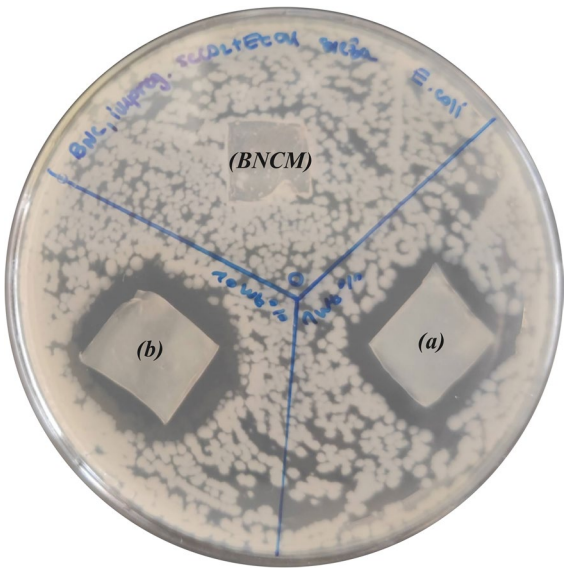

Fig. 7 Inhibition zone against G- *E. coli* by BNCMs enriched with (a) 1 wt% and (b) 10 wt% $scCO_2$ + EtOH ASE, determined by an agar diffusion assay (the concentration of *E. coli* was 1–5 × 10^6 CFU/mL) after 24 h of microbial growth at 37 ± 1 °C. Pure BNCM was applied as negative control

by BNCMs with differently concentrated solutions (1 and 10 wt%) of $scCO_2$ + EtOH ASE was small, resulting in 23–26 ± 1 mm and 16–18 ± 3 mm inhibition zones for *E. coli* and *S. aureus*, respectively.

The antibacterial activity of BNCMs enriched with ASE extracts was quantified further using the plate count method. The reduction rate (R) and corresponding log reduction factor (log R) were determined, along with the bactericidal/killing effect for both G- *E. coli* (Fig. 8a) and G + *S. aureus* (Fig. 8b) bacteria, as associated with inflammatory-related skin diseases (Madawi et al. 2023). Regarding the results presented in Fig. 8, all the BNCMs enriched with ASE exhibited a decrease in bacterial population after 24 h of exposure.

The highest, 100% reduction against G- *E. coli,* was attained using 10 wt% SOX-EtOH ASE (log R 2.33) and both $scCO_2$ + EtOH ASE (log R of 2.48 (1 wt%) and 2.56 (10 wt%), respectively) BNCMs, followed by 85% reduction using 10 wt% US-H_2O ASE (log R 0.94). A strong bactericidal effect was also detected for the mentioned BNCMs. The BNCMs with 1 wt% US-H_2O ASE resulted in a lower bacteriostatic potential (i.e., the bacterial strain survived, but did not reproduce) with minor bactericidal effects (72.04% production rate and log reduction of 0.55). *E. coli* was the most resistant to the addition of BNCMs modified with 1 wt% SOX-EtOH ASE, which resulted in around a 22.22% reduction rate, log reduction of 0.1 and 18.42% killing efficiency. The release of 1wt% SOX-EtOH ASE resulted in 0.26 mg/mL, while the minimum inhibitory concentrations (MIC_{90}) value for SOX-EtOH ASE against *E. coli* was determined at 0.28 mg/mL, which is the main reason for the lower bactericidal and bacteriostatic activity.

In the case of the G + *S. aureus*, BNCMs enriched with 10 wt% of SOX-EtOH and $scCO_2$ + EtOH ASE, a strong bactericidal effect was detected, which was confirmed with a 100% reduction of the bacterial cells and log reduction of 1.95. This is associated with the hydrodynamically smallest (0.1 µm) and well homogenized extract particles, as well as the relatively high

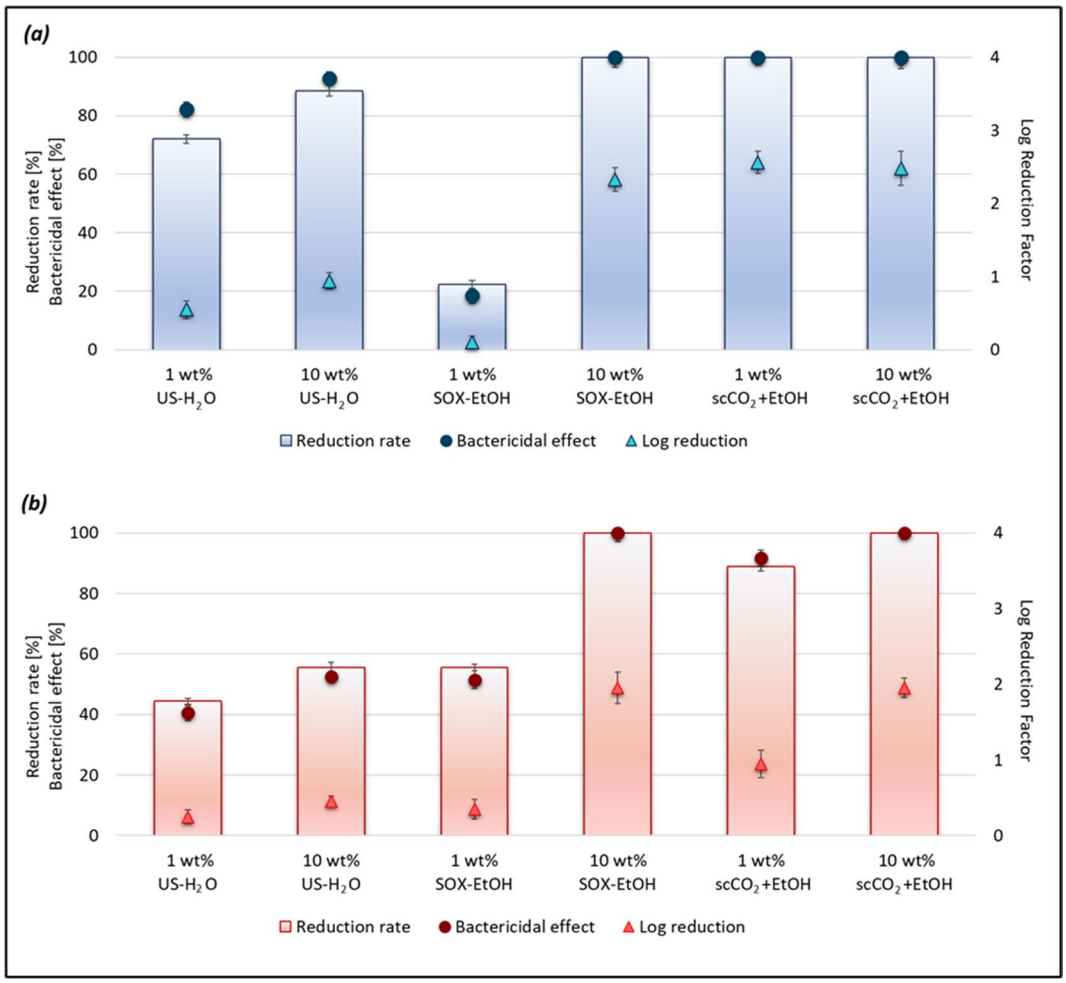

Fig. 8 Bacterial reduction rate, bactericidal effect, and log reduction of BNCMs enriched with US-H_2O, SOX-EtOH, and $scCO_2$ + EtOH ASE of different concentrations on (**a**) G- *E. coli* and (**b**) G + *S. aureus* determined by the plate count method (the concentration of both microorganisms was $1–5 \times 10^6$ CFU/mL) after 24 h of microbial growth

(484.91%) SW, as small particles can easily penetrate through the outermost layer of the bacterial cell envelope and thus contribute to a better antibacterial effect. BNCMs modified with 1 wt% $scCO_2$ + EtOH ASE exhibited somewhat lower bacteriostatic (88.89%) and bactericidal (88.89%) effects, corresponding to a log reduction of 0.95. Comparatively, BNCMs enriched with 1 wt% US-H_2O, 1 wt% SOX-EtOH, or 10 wt% US-H_2O ASE resulted to about half less effective bacterial reduction (44.39–55.62%) and killing efficiency (40.51–52.53%), with a log reduction of 0.25–0.45. Therefore, they can be considered as materials with minor bactericidal and bacteriostatic effects against *S. aureus*. The results correspond with the release studies, and relate with the MIC_{90} values determined in our previous study (Kupnik et al. 2023). The MIC_{90} for US-H_2O ASE was determined at 2.78 mg/mL, while the release of US-H_2O extracts after 24 h was 0.27 and 2.71 mg/mL for 1 and 10 wt%, respectively.

The extraction method has a significant influence on the content of biologically active compounds present in ASE, and, consequently, their bioactivity (Alexandre et al. 2018). Compared to UE and SE, SFE enables faster, near-ambient temperature, more sustainable and green extraction, which results in the recovery of pure biologically active extracts (Brglez Mojzer et al. 2016). Phytochemical screening of the

ASE exhibited the existence of different secondary metabolites, like alkaloids, flavonoids, phenolics, saponins, and tannins, and is well-documented in the literature (Setyawan et al. 2021; da Silva et al. 2022; Bangar et al. 2022; Nyakang'i et al. 2023). Differing bioactive compounds show distinctive modes of actions in the case of antimicrobial activity. For example, alkaloids interact with microbial DNA in order to promote antimicrobial action, while flavonoids disrupt bacterial cell walls, as they have the ability to form complexes with extracellular/soluble proteins of microbes. On the other hand, phenolics and tannins can bind to bacterial cell wall receptors, inhibit the enzymes which are required for cellular metabolism, and cause membrane disruption (Singh 2017; Wink 2022). In this manner, it is clear that the various phytochemicals in ASE contribute synergistically to imparting antibacterial activity.

The observed differences in antibacterial activity between different ASEs may thus be related to the extraction method and the resulting bioactive substances, the amount and availability of bioactive ASE on the surface of BNCMs, the release properties of the BNCMs, as well as the hydrodynamic size of the ASEs and their surface chemistry (Kokol et al. 2023a), which are crucial for their interaction with the bacteria outer cell layer and cell damage (Malanovic and Lohner 2016; Pajerski et al. 2020). The G- bacteria are composed of the inner cytoplasmic membrane, a thin peptidoglycan cell wall, and an outer membrane containing lipopolysaccharides. Contrarily, G + bacteria lack the protective outer membrane, as they consist only of the inner cytoplasmic membrane and a thick peptidoglycan cell wall (Rajagopal and Walker 2017; Rojas et al. 2018). In general, G + bacteria are known as more susceptible to the addition of antibacterial agents. However, the outer membrane of G- bacteria is permeable to small molecules due to porin channels, and impermeable to large molecules (Kokol et al. 2023b). Differently structured and large ASEs thus play an important role in the interaction with the outermost layer of the bacterial cell envelope, which may affect cell interaction and sensitivity to various ASEs.

Zeta potential (ZP) is a measure of the magnitude of the electrostatic attraction (or charge), or the repulsion between the functional groups or particle surfaces (Liu et al. 2023). The ZP of avocado seed ingredients in the range between -49.7 and -23.3 mV was evaluated (Sánchez-Quezada et al. 2023), which is in accordance with the ZP of the ASE extracted in our study, determined as average values in between -34.3 to -22.2 mV (see Table 2). In addition, bacterial surface charge, an electrochemical property of the cell surface, has often been described with ZP, and the net surface charge for most bacteria is negative. The average ZP for *S. aureus* and *E. coli* were found to be around -35.6 and -44.2 mv, respectively (Halder et al. 2015). Bacterial exposure to the antibacterial agents may be governed by electrostatic interactions, which can result in a ZP change. Two main reasons for altering ZP are possible, bacterial injury, or binding of the antibacterial agent to the bacterial surface (Ferreyra Maillard et al. 2021). These assumptions are supported by many researches including positively and negatively charged substances (Lopez-Romero et al. 2015; Ong et al. 2019; Ferreyra Maillard et al. 2019; 2021). As ASE are negatively charged, the resulting ZP of bacteria are probably shifted to more negative values. On that point, accumulation on the bacterial surface is the first step to cause bacterial injury. Regardless of the direction of ZP change, the addition of ASE affects cellular physiology, thus leading to the bacterial growth inhibition and/or cell death (Ferreyra Maillard et al. 2021). The more noticeable changes in ZP correlate with higher antibacterial activity (Ong et al. 2019), which is in line with the results observed for ASE. SOX-EtOH ASE and $scCO_2$ + EtOH ASE resulted in more negative ZP, leading to more intense lowering of ZP for *E. coli* and *S. aureus,* exhibiting better antibacterial efficiency in comparison with US-H_2O ones.

As already demonstrated well, the antibacterial properties of materials increase when prepared in the form of nanoparticles, as a large specific surface and the availability of a higher number of surface atoms can enhance their bioactivity (Shameli et al. 2011). Herein, a distinct difference was observed in the analyzed hydrodynamic sizes. Again, SOX-EtOH ASE and $scCO_2$ + EtOH ASE exhibited more than 11.7 times lower hydrodynamic size (approx. 100 nm) compared to US-H_2O ASE (i.e., 1340.7 nm). Consequently, ASE particles accumulated on the bacterial surface, the cell wall was disrupted and their leaching began into the highly permeable plasma (Khurana et al. 2014). On the other hand, the average particle size of the US-H_2O extract was higher, therefore, the interaction between the bacterial cell and the US-H_2O

ASE particles was limited severely, causing lower reduction of bacterial growth, and/or death. Additionally, PDI visualizes particle size distribution, and as the PDI value is lower, the uniformity degree is higher (Sitti et al. 2018). As the PDI of SOX-EtOH ASE and $scCO_2$ + EtOH ASE were significantly low (i.e., 0.17 and 0.14, respectively), indicating monodisperse samples, the production was expected of more homogeneous biocomposites. However, the PDI of US-H_2O ASE was higher (i.e., 0.65), indicating its poor uniformity and polydispersity. An inhomogeneous penetration and attachment of US-H_2O ASE may be the main reason for the interpretation of its lower antibacterial efficacy against G- *E. coli* and G+*S. aureus* compared to the other two ASEs, which is also in line with the results from the ZP values, hydrodynamic size and PDI of ASEs.

In addition, it is important to note that PDI values below 0.2 are acceptable in practise for polymer-based nanoparticle materials, while, in drug delivery, PDI values of 0.3 or below are considered as acceptable (Danaei et al. 2018). Hence, SOX-EtOH and $scCO_2$ + EtOH ASE are applicable for incorporation into polymer-based nanomaterials, and suitable for further applications in drug delivery with antibacterial effect.

Conclusions

In the presented study, an HS fermentation medium modified with 4 w/v% of sucrose and 2 w/v% of peptone at an initial pH value of 6.0 was proved to be an optimal medium for BNCMs` production with a high degree of crystallinity (up to 83%) using *K. hansenii* (DSM 5602). For the first time, the composites of BNCMs enriched with antimicrobially active ASE, extracted by different methods, were studied for applications in the health sector. Although all BNCMs enriched with ASE exerted growth reduction or complete inhibition of G- *E. coli* and G+*S. aureus*, BNCMs enriched with SOX-EtOH ASE and $scCO_2$ + EtOH ASE showed excellent bacteriostatic (up to 100% reduction with a log reduction up to 2.56) and bactericidal (up to 100%) activity. Such activity can be attributed to the hydrodynamically smaller (0.1–0.11 µm), homogeneous and more surface negative (-33 mV) ASE particles in the latter, favorable for interactions with the bacteria, and, as such, also suitable for applications in the delivery of antibacterial compounds. On the other hand, high swelling (up to 530%) and water retention properties demonstrated the ASE-enriched BNCMs suitability for versatile applications in biomedicine, cosmetics, and pharmacy related with skin regenerative medicine and wound healing. The biotechnological process of obtaining BNCMs should also be taken into consideration to be more efficient, what could happen due to alternative sources of carbon for BNCMs biosynthesis. However, the utilization of avocado seeds` waste thus enables and encompasses a broader strategy towards a circular economy that can be converted into sustainable value-added products.

Acknowledgments The authors acknowledge the use of research equipment for the production of biological substances and their detection, procured within the project "Upgrading national research infrastructures—RIUM", which was co-financed by the Republic of Slovenia, the Ministry of Higher Education, Science and Innovation, and the European Union from the European Regional Development Fund and the "System of downstream processes for performance of obtaining biological substances" (Package 21, ARIS).

Author contributions Conceptualization, M. L., M.P., K.K. and V.K.; methodology, M.L., M.P., K.K. and V.K..; formal analysis, K.K.; data curation, K.K..; writing—original draft preparation, K.K..; writing—review, M.L., M.P., V.K., and Z.K..; writing—editing, K.K.; visualization, K.K..; supervision, M.L., M.P. and V.K.; funding acquisition, M.L., V.K. and Z.K. All the authors have read and approved the final version of the manuscript.

Funding This research was supported by the Slovenian Research and Innovation Agency (ARIS) within the frame of Program P2-0046 (Separation Processes and Production Design), P2-0424 (Design of novel nano/material properties & applications), Project No. J2-3037 (Bionanotechnology as a tool for stabilization and applications of bioactive substances from natural sources), L2-4430 (Production, Isolation and Formulation of Health Beneficial Substances from*Helichrysum italicumfor Applications in the Cosmetic Industry), project BI-TR/22-24-04 "Enzyme immobilization techniques for efficient removal of antibiotics in wastewater" and Young Researcher ARIS Fellowship Contract No. 2187/FS-2019.*

Data availability Data is available upon reasonable request to authors.

Declarations

Ethical approval This study does not include any studies conducted by any author on human participants or animals. The authors claim the compliance with the ethical standards.

Competing interests The authors declare no competing interests.

References

Aleshina LA, Gladysheva EK, Budaeva VV, Golubev DS, Skiba EA, Sakovich GV (2019) X-ray diffraction study of bacterial nanocellulose produced by medusomyces Gisevii Sa-12 cultured in enzymatic hydrolysates of miscanthus. Crystallogr Rep 64(6):914–919. https://doi.org/10.1134/S1063774519060026

Alexandre EMC, Moreira SA, Castro LMG, Pintado M, Saraiva JA (2018) Emerging technologies to extract high added value compounds from fruit residues: Sub/supercritical, ultrasound-, and enzyme-assisted extractions. Food Rev Int 34(6):581–612. https://doi.org/10.1080/87559129.2017.1359842

Amorim JDP, Nascimento HA, Silva Junior CJG, Medeiros ADM, Silva IDL, Costa AFS, Vinhas GM, Sarubbo LA (2022) Obtainment of bacterial cellulose with added propolis extract for cosmetic applications. Polym Eng Sci 62(2):565–575. https://doi.org/10.1002/pen.25868

Atalla RH, VanderHart DL (1984) Native cellulose: a composite of two distinct crystalline forms. Science 223(4633):283–285. https://doi.org/10.1126/science.223.4633.283

Auta R, Adamus G, Kwiecien M, Radecka I, Hooley P (2017) Production and characterization of bacterial cellulose before and after enzymatic hydrolysis. AJB 16(10):470–482. https://doi.org/10.5897/AJB2016.15486

Azarmi R, Ashjaran A, Nourbakhsh S, Talebian A (2022) Plant extract delivery and antibacterial properties of nano bacterial cellulose in the presence of dendrimer, chitosan, and herbal materials. J Ind Text 52:1–23. https://doi.org/10.1177/15280837221121977

Bangar SP, Dunno K, Dhull SB, Kumar Siroha A, Changan S, Maqsood S, Rusu AV (2022) Avocado seed discoveries: Chemical composition, biological properties, and industrial food applications. Food Chem: X 16:100507. https://doi.org/10.1016/j.fochx.2022.100507

Bhattacharjee R, Negi A, Bhattacharya B, Dey T, Mitra P, Preetam S, Kumar L, Kar S, Das SS, Iqbal D, Kamal M, Alghofaili F, Malik S, Dey A, Jha SK, Ojha S, Paiva-Santos AC, Kesari KK, Jha NK (2023) Nanotheranostics to target antibiotic-resistant bacteria: strategies and applications. OpenNano 11:100138. https://doi.org/10.1016/j.onano.2023.100138

Bimmer M, Reimer M, Klingl A, Ludwig C, Zollfrank C, Liebl W, Ehrenreich A (2023) Analysis of cellulose synthesis in a high-producing acetic acid bacterium Komagataeibacter hansenii. Appl Microbiol Biotechnol 107(9):2947–2967. https://doi.org/10.1007/s00253-023-12461-z

Bodea IM, Cătunescu GM, Pop CR, Fiț NI, David AP, Dudescu MC, Stănilă A, Rotar AM, Beteg FI (2022) Antimicrobial properties of bacterial cellulose films enriched with bioactive herbal extracts obtained by microwave-assisted extraction. Polymers (Basel) 14(7):1435. https://doi.org/10.3390/polym14071435

Bogireddy N, Agarwal V (2019) Persea americana seed extract mediated gold nanoparticles for mercury(II)/iron(III) sensing, 4- nitrophenol reduction, and organic dye degradation †. RSC Adv 9:39834. https://doi.org/10.1039/c9ra08233f

Brglez Mojzer E, Knez Hrnčič M, Škerget M, Knez Ž, Bren U (2016) Polyphenols: extraction methods, antioxidative action, bioavailability and anticarcinogenic effects. Molecules 21(7):901. https://doi.org/10.3390/molecules21070901

Campos DA, Gómez-García R, Vilas-Boas AA, Madureira AR, Pintado MM (2020) Management of fruit industrial by-products—a case study on circular economy approach. Molecules 25(2):320. https://doi.org/10.3390/molecules25020320

Cielecka I, Ryngajłło M, Bielecki S (2020) BNC biosynthesis with increased productivity in a newly designed surface air-flow bioreactor. Appl Sci 10(11):3850. https://doi.org/10.3390/app10113850

Cielecka I, Ryngajłło M, Maniukiewicz W, Bielecki S (2021) Highly stretchable bacterial cellulose produced by Komagataeibacter hansenii SI1. Polymers 13(24):4455. https://doi.org/10.3390/polym13244455

Czaja W, Krystynowicz A, Bielecki S, Brown RM (2006) Microbial cellulose—the natural power to heal wounds. Biomaterials 27(2):145–151. https://doi.org/10.1016/j.biomaterials.2005.07.035

da Silva GG, Pimenta LPS, Melo JOF, Mendonça H de OP, Augusti R, Takahashi JA (2022) Phytochemicals of avocado residues as potential acetylcholinesterase inhibitors, antioxidants, and neuroprotective agents. Molecules 27(6):1892.https://doi.org/10.3390/molecules27061892

Danaei M, Dehghankhold M, Ataei S, Hasanzadeh Davarani F, Javanmard R, Dokhani A, Khorasani S, Mozafari MR (2018) Impact of particle size and polydispersity index on the clinical applications of lipidic nanocarrier systems. Pharmaceutics 10(2):57. https://doi.org/10.3390/pharmaceutics10020057

Dayal MS, Goswami N, Sahai A, Jain V, Mathur G, Mathur A (2013) Effect of media components on cell growth and bacterial cellulose production from Acetobacter aceti MTCC 2623. Carbohydr Polym 94(1):12–16. https://doi.org/10.1016/j.carbpol.2013.01.018

Digel I, Akimbekov N, Rogachev E, Pogorelova N (2023) Bacterial cellulose produced by Medusomyces gisevii on glucose and sucrose: biosynthesis and structural

properties. Cellulose 30(18):11439–11453. https://doi.org/10.1007/s10570-023-05592-z

Domínguez MP, Araus K, Bonert P, Sánchez F, San Miguel G, Toledo M (2016) The avocado and its waste: an approach of fuel potential/application. In: Lefebvre G, Jiménez E, Cabañas B (eds) Environment, energy and climate change II: energies from new resources and the climate change. Springer International Publishing, Cham, pp 199–223

Fan X, Gao Y, He W, Hu H, Tian M, Wang K, Pan S (2016) Production of nano bacterial cellulose from beverage industrial waste of citrus peel and pomace using Komagataeibacter xylinus. Carbohydr Polym 151:1068–1072. https://doi.org/10.1016/j.carbpol.2016.06.062

Fang L, Catchmark JM (2014) Structure characterization of native cellulose during dehydration and rehydration. Cellulose 21(6):3951–3963. https://doi.org/10.1007/s10570-014-0435-8

Fatima A, Yasir S, Ul-Islam M, Kamal T, Ahmad MdW, Abbas Y, Manan S, Ullah MW, Yang G (2022) Ex situ development and characterization of green antibacterial bacterial cellulose-based composites for potential biomedical applications. Adv Compos Hybrid Mater 5(1):307–321. https://doi.org/10.1007/s42114-021-00369-z

Ferreyra Maillard APV, Gonçalves S, Santos NC, López de Mishima BA, Dalmasso PR, Hollmann A (2019) Studies on interaction of green silver nanoparticles with whole bacteria by surface characterization techniques. Biochim Biophys Acta Biomembr 1861(6):1086–1092. https://doi.org/10.1016/j.bbamem.2019.03.011

Ferreyra Maillard APV, Espeche JC, Maturana P, Cutro AC, Hollmann A (2021) Zeta potential beyond materials science: Applications to bacterial systems and to the development of novel antimicrobials. Biochim Biophys Acta Biomembr 1863(6):183597. https://doi.org/10.1016/j.bbamem.2021.183597

Fontana JD, De Souza AM, Fontana CK, Torriani IL, Moreschi JC, Gallotti BJ, De Souza SJ, Narcisco GP, Bichara JA, Farah LFX (1990) Acetobacter cellulose pellicle as a temporary skin substitute. Appl Biochem Biotechnol 24(1):253–264. https://doi.org/10.1007/BF02920250

French AD (2014) Idealized powder diffraction patterns for cellulose polymorphs. Cellulose 21(2):885–896. https://doi.org/10.1007/s10570-013-0030-4

French AD, Santiago Cintrón M (2013) Cellulose polymorphy, crystallite size, and the Segal crystallinity index. Cellulose 20(1):583–588. https://doi.org/10.1007/s10570-012-9833-y

George J, Sajeevkumar VA, Kumar R, Ramana KV, Sabapathy SN, Bawa AS (2008) Enhancement of thermal stability associated with the chemical treatment of bacterial (Gluconacetobacter xylinus) cellulose. J Appl Polym Sci 108(3):1845–1851. https://doi.org/10.1002/app.27802

Ghozali M, Meliana Y, Chalid M (2021) Synthesis and characterization of bacterial cellulose by Acetobacter xylinum using liquid tapioca waste. Mater Today: Proc 44:2131–2134. https://doi.org/10.1016/j.matpr.2020.12.274

Gupte Y, Kulkarni A, Raut B, Sarkar P, Choudhury R, Chawande A, Kumar GRK, Bhadra B, Satapathy A, Das G, Vishnupriya B, Dasgupta S (2021) Characterization of nanocellulose production by strains of Komagataeibacter sp. isolated from organic waste and Kombucha. Carbohydr Polym 266:118176. https://doi.org/10.1016/j.carbpol.2021.118176

Güzel M, Akpınar Ö (2020) Preparation and characterization of bacterial cellulose produced from fruit and vegetable peels by Komagataeibacter hansenii GA2016. Int J Biol Macromol 162:1597–1604. https://doi.org/10.1016/j.ijbiomac.2020.08.049

Halder S, Yadav KK, Sarkar R, Mukherjee S, Saha P, Haldar S, Karmakar S, Sen T (2015) Alteration of Zeta potential and membrane permeability in bacteria: a study with cationic agents. Springerplus 4:672. https://doi.org/10.1186/s40064-015-1476-7

Heydorn RL, Lammers D, Gottschling M, Dohnt K (2023) Effect of food industry by-products on bacterial cellulose production and its structural properties. Cellulose 30(7):4159–4179. https://doi.org/10.1007/s10570-023-05097-9

Hu W, Chen S, Yang J, Li Z, Wang H (2014) Functionalized bacterial cellulose derivatives and nanocomposites. Carbohydr Polym 101:1043–1060. https://doi.org/10.1016/j.carbpol.2013.09.102

Illa MP, Sharma CS, Khandelwal M (2019) Tuning the physiochemical properties of bacterial cellulose: effect of drying conditions. J Mater Sci 54(18):12024–12035. https://doi.org/10.1007/s10853-019-03737-9

Indrianingsih AW, Rosyida VT, Apriyana W, Hayati SN, Darsih C, Nisa K, Ratih D (2020) Antioxidant and antibacterial properties of bacterial cellulose— Indonesian plant extract composites for mask sheet. J App Pharm Sci 10(7):037–042. https://doi.org/10.7324/JAPS.2020.10705

Islam M, Khan T, Park J (2012) Water holding and release properties of bacterial cellulose obtained by in situ and ex situ modification. Carbohydr Polym 88:596–603. https://doi.org/10.1016/j.carbpol.2012.01.006

Jimenez P, Garcia P, Quitral V, Vasquez K, Parra-Ruiz C, Reyes-Farias M, Garcia-Diaz DF, Robert P, Encina C, Soto-Covasich J (2021) Pulp, leaf, peel and seed of avocado fruit: a review of bioactive compounds and healthy benefits. Food Rev Intl 37(6):619–655. https://doi.org/10.1080/87559129.2020.1717520

Jipa IM, Stoica-Guzun A, Stroescu M (2012) Controlled release of sorbic acid from bacterial cellulose based mono and multilayer antimicrobial films. LWT 47(2):400–406. https://doi.org/10.1016/j.lwt.2012.01.039

Kalkhoran AHZ, Naghib SM, Vahidi O, Rahmanian M (2018) Synthesis and characterization of graphene-grafted gelatin nanocomposite hydrogels as emerging drug delivery systems. Biomed Phys Eng Express 4(5):055017. https://doi.org/10.1088/2057-1976/aad745

Kamal T, Ul-Islam M, Khan SB, Bakhsh EM, Chani MTS (2022) Development of plant extract impregnated bacterial cellulose as a green antimicrobial composite for potential biomedical applications. Ind Crops Prod 187:115337. https://doi.org/10.1016/j.indcrop.2022.115337

Keshk SMAS, Sameshima K (2005) Evaluation of different carbon sources for bacterial cellulose production. AJB 4(6):478–482

Khamrai M, Banerjee SL, Kundu PP (2017) Modified bacterial cellulose based self-healable polyelectrolyte film for wound dressing application. Carbohydr Polym 174:580–590. https://doi.org/10.1016/j.carbpol.2017.06.094

Khine YY, Stenzel MH (2020) Surface modified cellulose nanomaterials: a source of non-spherical nanoparticles for drug delivery. Mater Horiz 7(7):1727–1758. https://doi.org/10.1039/C9MH01727E

Khurana C, Vala AK, Andhariya N, Pandey OP, Chudasama B (2014) Antibacterial activity of silver: the role of hydrodynamic particle size at nanoscale. J Biomed Mater Res A 102(10):3361–3368. https://doi.org/10.1002/jbm.a.35005

Kokol V, Kos M, Vivod V, Gunde-Cimerman N (2023a) Cationised fibre-based cellulose multi-layer membranes for sterile and high-flow bacteria retention and inactivation. Membranes 13(3):284. https://doi.org/10.3390/membranes13030284

Kokol V, Novak S, Kononenko V, Kos M, Vivod V, Gunde-Cimerman N, Drobne D (2023b) Antibacterial and degradation properties of dialdehyded and aminohexamethylated nanocelluloses. Carbohydr Polym 311:120603. https://doi.org/10.1016/j.carbpol.2023.120603

Kupnik K, Primožič M, Kokol V, Leitgeb M (2020) Nanocellulose in drug delivery and antimicrobially active materials. Polymers 12(12):2825. https://doi.org/10.3390/polym12122825

Kupnik K, Primožič M, Knez Ž, Leitgeb M (2021a) Antimicrobial efficiency of aloe arborescens and aloe barbadensis natural and commercial products. Plants 10(1):92. https://doi.org/10.3390/plants10010092

Kupnik K, Primožič M, Vasić K, Knez Ž, Leitgeb M (2021) A comprehensive study of the antibacterial activity of bioactive juice and extracts from pomegranate (Punica granatum L.) peels and seeds. Plants 10(8):1554. https://doi.org/10.3390/plants10081554

Kupnik K, Primožič M, Kokol V, Knez Ž, Leitgeb M (2023) Enzymatic, antioxidant, and antimicrobial activities of bioactive compounds from avocado (Persea americana L.) seeds. Plants 12(5):1201. https://doi.org/10.3390/plants12051201

Lazarini SC, de Aquino R, Amaral AC, Corbi FCA, Corbi PP, Barud HS, Lustri WR (2016) Characterization of bilayer bacterial cellulose membranes with different fiber densities: a promising system for controlled release of the antibiotic ceftriaxone. Cellulose 23(1):737–748. https://doi.org/10.1007/s10570-015-0843-4

Leite JJG, Brito ÉHS, Cordeiro RA, Brilhante RSN, Sidrim JJC, Bertini LM, de Morais SM, Rocha MFG (2009) Chemical composition, toxicity and larvicidal and antifungal activities of Persea americana (avocado) seed extracts. Rev Soc Bras Med 42:110–113. https://doi.org/10.1590/S0037-86822009000200003

Li Y-T, Lin S-B, Chen L-C, Chen H-H (2017) Antimicrobial activity and controlled release of nanosilvers in bacterial cellulose composites films incorporated with montmorillonites. Cellulose 24(11):4871–4883. https://doi.org/10.1007/s10570-017-1487-3

Lima HLS, Nascimento ES, Andrade FK, Brígida AIS, Borges MF, Cassales AR, Muniz CR, Souza M de SM, Morais JPS, Rosa M de F (2017) Bacterial cellulose production by *Komagataeibacter hansenii* ATCC 23769 using Sisal juice - an agroindustry waste. Braz J Chem Eng 34:671–680.https://doi.org/10.1590/0104-6632.20170343s20150514

Lin S-P, Loira Calvar I, Catchmark JM, Liu J-R, Demirci A, Cheng K-C (2013a) Biosynthesis, production and applications of bacterial cellulose. Cellulose 20(5):2191–2219. https://doi.org/10.1007/s10570-013-9994-3

Lin W-C, Lien C-C, Yeh H-J, Yu C-M, Hsu S (2013b) Bacterial cellulose and bacterial cellulose–chitosan membranes for wound dressing applications. Carbohydr Polym 94(1):603–611. https://doi.org/10.1016/j.carbpol.2013.01.076

Liu M, Liang J, Jing C, Yue Y, Xia Y, Yuan Y, Yue T (2023) Preparation and characterization of Lycium Barbarum seed oil Pickering emulsions and evaluation of antioxidant activity. Food Chem 405:134906. https://doi.org/10.1016/j.foodchem.2022.134906

Lopez-Romero JC, González-Ríos H, Borges A, Simões M (2015) Antibacterial effects and mode of action of selected essential oils components against Escherichia coli and staphylococcus aureus. Evid Based Complement Alternat Med 2015:795435. https://doi.org/10.1155/2015/795435

Madawi EA, Al Jayoush AR, Rawas-Qalaji M, Thu HE, Khan S, Sohail M, Mahmood A, Hussain Z (2023) Polymeric nanoparticles as tunable nanocarriers for targeted delivery of drugs to skin tissues for treatment of topical skin diseases. Pharmaceutics 15(2):657. https://doi.org/10.3390/pharmaceutics15020657

Malanovic N, Lohner K (2016) Gram-positive bacterial cell envelopes: The impact on the activity of antimicrobial peptides. Biochim Biophys Acta Biomembr 1858(5):936–946. https://doi.org/10.1016/j.bbamem.2015.11.004

Mbituyimana B, Liu L, Ye W, Ode Boni BO, Zhang K, Chen J, Thomas S, Vasilievich RV, Shi Z, Yang G (2021) Bacterial cellulose-based composites for biomedical and cosmetic applications: research progress and existing products. Carbohydr Polym 273:118565. https://doi.org/10.1016/j.carbpol.2021.118565

Mikkelsen D, Flanagan BM, Dykes GA, Gidley MJ (2009) Influence of different carbon sources on bacterial cellulose production by Gluconacetobacter xylinus strain ATCC 53524. J Appl Microbiol 107(2):576–583. https://doi.org/10.1111/j.1365-2672.2009.04226.x

Mocanu A, Isopencu G, Busuioc C, Popa O-M, Dietrich P, Socaciu-Siebert L (2019) Bacterial cellulose films with ZnO nanoparticles and propolis extracts: Synergistic antimicrobial effect. Sci Rep 9(1):17687. https://doi.org/10.1038/s41598-019-54118-w

Mohamad S, Abdullah LC, Jamari SS, Al Edrus SSO, Aung MM, Mohamad SFS (2022) Influence of drying method on the crystal structure and thermal property of oil palm frond juice-based bacterial cellulose. J Mater Sci 57(2):1462–1473. https://doi.org/10.1007/s10853-021-06685-5

Mohammadkazemi F, Azin M, Ashori A (2015a) Production of bacterial cellulose using different carbon sources and culture media. Carbohydr Polym 117:518–523. https://doi.org/10.1016/j.carbpol.2014.10.008

Mohammadkazemi F, Doosthoseini K, Azin M (2015) Effect of ethanol and medium on bacterial cellulose (BC) production by gluconacetobacter xylinus (PTCC 1734). Cellulose Chem Technol 49(5–6):455–462fan

Mohite BV, Salunke BK, Patil SV (2013) Enhanced production of bacterial cellulose by using gluconacetobacter hansenii NCIM 2529 strain under shaking conditions. Appl

Biochem Biotechnol 169(5):1497–1511. https://doi.org/10.1007/s12010-013-0092-7

Neves EZ, Kumineck Junior SR, Katrucha GP, Silveira VF, Silveira MLL, Pezzin APT, Schneider AL dos S, Garcia MCF, Apati GP (2022) Development of bacterial cellulose membranes incorporated with plant extracts. Macromol Symp 406(1):2200031https://doi.org/10.1002/masy.202200031

Nwaoguikpe R, Braide W, Ujowundu C (2011) Biochemical composition and antimicrobial activities of seed extracts of avocado (Persea americana). J Microbiol Antimicrob 3(7):184–190. https://doi.org/10.5897/JMA.9000014

Nyakang'i CO, Marete E, Ebere R, Arimi JM (2023) Physicochemical properties of avocado seed extract model beverages and baked products incorporated with avocado seed powder. Int J Food Sci 2023:6860806. https://doi.org/10.1155/2023/6860806

Oliveira RN, Mancini MC, Oliveira FCS de, Passos TM, Quilty B, Thiré RM da SM, McGuinness GB (2016) FTIR analysis and quantification of phenols and flavonoids of five commercially available plants extracts used in wound healing. Matéria (Rio J) 21:767–779.https://doi.org/10.1590/S1517-707620160003.0072

Ong TH, Chitra E, Ramamurthy S, Ling CCS, Ambu SP, Davamani F (2019) Cationic chitosan-propolis nanoparticles alter the zeta potential of S, epidermidis, inhibit biofilm formation by modulating gene expression and exhibit synergism with antibiotics. PLOS One 14(2):e0213079. https://doi.org/10.1371/journal.pone.0213079

Pajerski W, Duch J, Ochonska D, Golda-Cepa M, Brzychczy-Wloch M, Kotarba A (2020) Bacterial attachment to oxygen-functionalized graphenic surfaces. Mater Sci Eng C 113:110972. https://doi.org/10.1016/j.msec.2020.110972

Perużyńska M, Nowak A, Birger R, Ossowicz-Rupniewska P, Konopacki M, Rakoczy R, Kucharski Ł, Wenelska K, Klimowicz A, Droździk M, Kurzawski M (2023) Anticancer properties of bacterial cellulose membrane containing ethanolic extract of Epilobium angustifolium L. Front Bioeng Biotechnol 11:1133345. https://doi.org/10.3389/fbioe.2023.1133345

Pinto RJB, Neves MC, Neto CP, Trindade T, Pinto RJB, Neves MC, Neto CP, Trindade T (2012) Composites of cellulose and metal nanoparticles. In: nanocomposites - new trends and developments. IntechOpen, pp 73–96. https://doi.org/10.5772/50553

Pooja R, Vadodaria K, Vidhya S (2019) Synthesis of bacterial cellulose and herbal extract for the development of wound dressing. Mater Today: Proc 15:284–293. https://doi.org/10.1016/j.matpr.2019.05.007

Pourramezan GZ, Roayaei AM, Qezelbash QR (2009) Optimization of culture conditions for bacterial cellulose production by acetobacter sp. 4B–2. Biotechnology 8:150–154. https://doi.org/10.3923/biotech.2009.150.154

Rabobank (2023) World avocado map 2023: global growth far from over. https://research.rabobank.com/far/en/sectors/fresh-produce/world-avocado-map-2023-global-growth-far-from-over.html. Accessed 5 Aug 2023

Rajagopal M, Walker S (2017) Envelope structures of gram-positive bacteria. Curr Top Microbiol Immunol 404:1–44. https://doi.org/10.1007/82_2015_5021

Rani MU, Appaiah A (2011) Optimization of culture conditions for bacterial cellulose production from Gluconacetobacter hansenii UAC09. Ann Microbiol 61(4):781–787. https://doi.org/10.1007/s13213-011-0196-7

Rodríguez FJ, Schlenger P, García-Valverde M (2016) Monitoring changes in the structure and properties of humic substances following ozonation using UV–Vis, FTIR and 1H NMR techniques. Sci Total Environ 541:623–637. https://doi.org/10.1016/j.scitotenv.2015.09.127

Rojas ER, Billings G, Odermatt PD, Auer GK, Zhu L, Miguel A, Chang F, Weibel DB, Theriot JA, Huang KC (2018) The outer membrane is an essential load-bearing element in Gram-negative bacteria. Nature 559(7715):617–621. https://doi.org/10.1038/s41586-018-0344-3

Ruka DR, Simon GP, Dean KM (2012) Altering the growth conditions of Gluconacetobacter xylinus to maximize the yield of bacterial cellulose. Carbohydr Polym 89(2):613–622. https://doi.org/10.1016/j.carbpol.2012.03.059

Sakthivel K, Periyasamy S, Hungund B (2016) Biosynthesis of bacterial cellulose and imparting antibacterial property through novel bio-agents. Res J Biotechnol 11(9):86–93

Sánchez-Quezada V, Gaytán-Martínez M, Recio I, Loarca-Piña G (2023) Avocado seed by-product uses in emulsion-type ingredients with nutraceutical value: Stability, cytotoxicity, nutraceutical properties, and assessment of in vitro oral-gastric digestion. Food Chem 421:136118. https://doi.org/10.1016/j.foodchem.2023.136118

Segal L, Creely JJ, Martin AE, Conrad CM (1959) An empirical method for estimating the degree of crystallinity of native cellulose using the x-ray diffractometer. Text Res J 29(10):786–794. https://doi.org/10.1177/004051755902901003

Setyawan HY, Sukardi S, Puriwangi CA (2021) Phytochemicals properties of avocado seed: a review. IOP Conf Ser: Earth Environ Sci 733(1):012090. https://doi.org/10.1088/1755-1315/733/1/012090

Shameli K, Ahmad MB, Zargar M, Yunus WMZW, Rustaiyan A, Ibrahim NA (2011) Synthesis of silver nanoparticles in montmorillonite and their antibacterial behavior. Int J Nanomedicine 6:581–590. https://doi.org/10.2147/IJN.S17112

Sharma C, Bhardwaj NK (2019) Bacterial nanocellulose: Present status, biomedical applications and future perspectives. Mater Sci Eng C-Mater Biol Appl 104:109963. https://doi.org/10.1016/j.msec.2019.109963

Shen R, Yang X, Lin D (2023) pH sensitive double-layered emulsions stabilized by bacterial cellulose nanofibers/soy protein isolate/chitosan complex enhanced the bioaccessibility of curcumin: In vitro study. Food Chem 402:134262. https://doi.org/10.1016/j.foodchem.2022.134262

Sheykhnazari S, Tabarsa T, Ashori A, Shakeri A, Golalipour M (2011) Bacterial synthesized cellulose nanofibers; effects of growth times and culture mediums on the structural characteristics. Carbohydr Polym 86(3):1187–1191. https://doi.org/10.1016/j.carbpol.2011.06.011

Shezad O, Khan S, Khan T, Park JK (2010) Physicochemical and mechanical characterization of bacterial cellulose produced with an excellent productivity in static conditions using a simple fed-batch cultivation strategy. Carbohydr Polym 82(1):173–180. https://doi.org/10.1016/j.carbpol.2010.04.052

Singh I (2017) Antimicrobials in higher plants: classification, mode of action and bioactivities. Chem Biol Lett 4(1):48–62

Singhsa P, Narain R, Manuspiya H (2018) Physical structure variations of bacterial cellulose produced by different Komagataeibacter xylinus strains and carbon sources in static and agitated conditions. Cellulose 25(3):1571–1581. https://doi.org/10.1007/s10570-018-1699-1

Sitti R, Sugita P, Ambarsari L, Rahayu D (2018) Antibacterial mangosteen (Garcinia mangostana Linn.) peel extract encapsulated in Chitosan. J Phys Conf Ser 1116:042037. https://doi.org/10.1088/1742-6596/1116/4/042037

Sperotto G, Stasiak LG, Godoi JPMG, Gabiatti NC, De Souza SS (2021) A review of culture media for bacterial cellulose production: complex, chemically defined and minimal media modulations. Cellulose 28(5):2649–2673. https://doi.org/10.1007/s10570-021-03754-5

Sulaeva I, Henniges U, Rosenau T, Potthast A (2015) Bacterial cellulose as a material for wound treatment: properties and modifications. A review. Biotechnol Adv 33(8):1547–1571. https://doi.org/10.1016/j.biotechadv.2015.07.009

Tang W, Jia S, Jia Y, Yang H (2010) The influence of fermentation conditions and post-treatment methods on porosity of bacterial cellulose membrane. World J Microbiol Biotechnol 26(1):125–131. https://doi.org/10.1007/s11274-009-0151-y

Taokaew S, Nunkaew N, Siripong P, Phisalaphong M (2014) Characteristics and anticancer properties of bacterial cellulose films containing ethanolic extract of mangosteen peel. J Biomater Sci Polym Ed 25(9):907–922. https://doi.org/10.1080/09205063.2014.913464

Treesuppharat W, Rojanapanthu P, Siangsanoh C, Manuspiya H, Ummartyotin S (2017) Synthesis and characterization of bacterial cellulose and gelatin-based hydrogel composites for drug-delivery systems. Biotechnol Rep 15:84–91. https://doi.org/10.1016/j.btre.2017.07.002

Ul-Islam M, Alhajaim W, Fatima A, Yasir S, Kamal T, Abbas Y, Khan S, Khan AH, Manan S, Ullah MW, Yang G (2023) Development of low-cost bacterial cellulose-pomegranate peel extract-based antibacterial composite for potential biomedical applications. Int J Biol Macromol 231:123269. https://doi.org/10.1016/j.ijbiomac.2023.123269

Ullah H, Santos HA, Khan T (2016) Applications of bacterial cellulose in food, cosmetics and drug delivery. Cellulose 23(4):2291–2314. https://doi.org/10.1007/s10570-016-0986-y

Ullah H, Badshah M, Mäkilä E, Salonen J, Shahbazi M-A, Santos HA, Khan T (2017) Fabrication, characterization and evaluation of bacterial cellulose-based capsule shells for oral drug delivery. Cellulose 24(3):1445–1454. https://doi.org/10.1007/s10570-017-1202-4

Ullah MW, Manan S, Kiprono SJ, Ul-Islam M, Yang G (2019) Synthesis, structure, and properties of bacterial cellulose. In: Nanocellulose. Wiley Ltd, pp 81–113

Urbina L, Corcuera MÁ, Gabilondo N, Eceiza A, Retegi A (2021) A review of bacterial cellulose: sustainable production from agricultural waste and applications in various fields. Cellulose 28(13):8229–8253. https://doi.org/10.1007/s10570-021-04020-4

Uzyol HK, Saçan MT (2017) Bacterial cellulose production by Komagataeibacter hansenii using algae-based glucose. Environ Sci Pollut Res Int 24(12):11154–11162. https://doi.org/10.1007/s11356-016-7049-7

Vigentini I, Fabrizio V, Dellacà F, Rossi S, Azario I, Mondin C, Benaglia M, Foschino R (2019) Set-up of bacterial cellulose production from the genus Komagataeibacter and its use in a gluten-free bakery product as a case study. Front Microbiol 10:1953. https://doi.org/10.3389/fmicb.2019.01953

Wada M, Okano T, Sugiyama J (2001) Allomorphs of native crystalline cellulose I evaluated by two equatoriald-spacings. J Wood Sci 47(2):124–128. https://doi.org/10.1007/BF00780560

Wang S-S, Han Y-H, Chen J-L, Zhang D-C, Shi X-X, Ye Y-X, Chen D-L, Li M (2018) Insights into bacterial cellulose biosynthesis from different carbon sources and the associated biochemical transformation pathways in Komagataeibacter sp. W1. Polymers 10(9):963. https://doi.org/10.3390/polym10090963

Wang J, Tavakoli J, Tang Y (2019) Bacterial cellulose production, properties and applications with different culture methods – a review. Carbohydr Polym 219:63–76. https://doi.org/10.1016/j.carbpol.2019.05.008

Wink M (2022) Current understanding of modes of action of multicomponent bioactive phytochemicals: potential for nutraceuticals and antimicrobials. Annu Rev Food Sci Technol 13(1):337–359. https://doi.org/10.1146/annurev-food-052720-100326

Yassine F, Bassil N, Chokr A, El Samrani A, Serghei A, Boiteux G, El Tahchi M (2016) Two-step formation mechanism of Acetobacter cellulosic biofilm: synthesis of sparse and compact cellulose. Cellulose 23(2):1087–1100. https://doi.org/10.1007/s10570-016-0884-3

Yi X, Cheng F, Wei X, Li H, Qian J, He J (2023) Bioinspired adhesive and self-healing bacterial cellulose hydrogels formed by a multiple dynamic crosslinking strategy for sealing hemostasis. Cellulose 30(1):397–411. https://doi.org/10.1007/s10570-022-04909-8

Zeng X, Small DP, Wan W (2011) Statistical optimization of culture conditions for bacterial cellulose production by Acetobacter xylinum BPR 2001 from maple syrup. Carbohydr Polym 85(3):506–513. https://doi.org/10.1016/j.carbpol.2011.02.034

Zeng M, Laromaine A, Feng W, Levkin PA, Roig A (2014) Origami magnetic cellulose: controlled magnetic fraction and patterning of flexible bacterial cellulose. J Mater Chem C 2(31):6312–6318. https://doi.org/10.1039/C4TC00787E

Zhou Q, Chen J, Jin B, Chu S, Peng R (2021) Modification of ZIF-8 on bacterial cellulose for an efficient selective capture of U(VI). Cellulose 28(9):5241–5256. https://doi.org/10.1007/s10570-021-03820-y